Appendix G

Seepage Analysis

December 2019

TABLE OF CONTENTS

LIST OF FIGURES

LIST OF TABLES

1 INTRODUCTION

This Appendix presents the seepage analysis of the Vale S.A. ("Vale") Córrego do Feijão Mine Dam I ("Dam I"). Seepage numerical modeling was performed to establish the saturated and unsaturated flow regime within the dam prior to failure and allowed an understanding of water flow and pore water pressure conditions in the dam during construction and at the time of failure. The numerical modeling was focused on the tailings impoundment and the upstream-constructed dam.

2 PROCEDURE

One-dimensional (1D) modeling was used to evaluate the effect of climatic change on near-surface suctions as well as to calculate net rainfall infiltration rates. Two-dimensional (2D) modeling was used for detailed calibration of the seepage model and to calculate pore water pressures during construction and as of the date of failure on January 25, 2019. A three-dimensional (3D) model was created to assess whether the results of the 2D model were consistent with the 2D calibration and to provide a 3D calibration, as well as construction pore water pressures. The 1D, 2D, and 3D seepage modeling and associated calibration utilized the computer softwares SVFLUX™, SVDESIGNER™, and SVSOILS™.

3 CLIMATE, RAINFALL, AND INFILTRATION

The climate regime at Dam I is classified as humid tropical with distinct wet and dry seasons. Characterization and analysis of rainfall was required to evaluate the water level, net infiltration, and seepage within Dam I.

3.1 Analysis of Rainfall Data

After tailings deposition ceased in July 2016, the water level would have been influenced primarily by the net rainfall infiltration into the tailings. Rainfall data were available from locations at or near the dam site, as described in Appendix C, including:

- Automated rainfall gauge F18 ("F18"), located approximately 1.4 kilometers (km) northwest of Dam I. Although the closest in location to Dam I, this gauge only had rainfall data beginning in March 2017 (i.e., covering approximately the last two years prior to the failure);

- Automated rainfall gauge F11 ("F11"), located approximately 18.6 km northeast of Dam I, which had rainfall data from January 2016 (i.e., approximately the last three years prior to the failure); and

- INMET Ibirité weather station, located approximately 15 km northeast of Dam I; the data used covered the period from 2008 to 2019.

Figure 1 shows the annual rainfall for the 10-year period from 2008-2009 to 2018-2019 at the INMET Ibirité weather station, plotted from July to June of the following year, so as not to split the wet season. The years from 2008-2009 to 2011-2012 were the wettest, with 2018-2019 being the next wettest, up 53% from the driest year in 2013-2014.

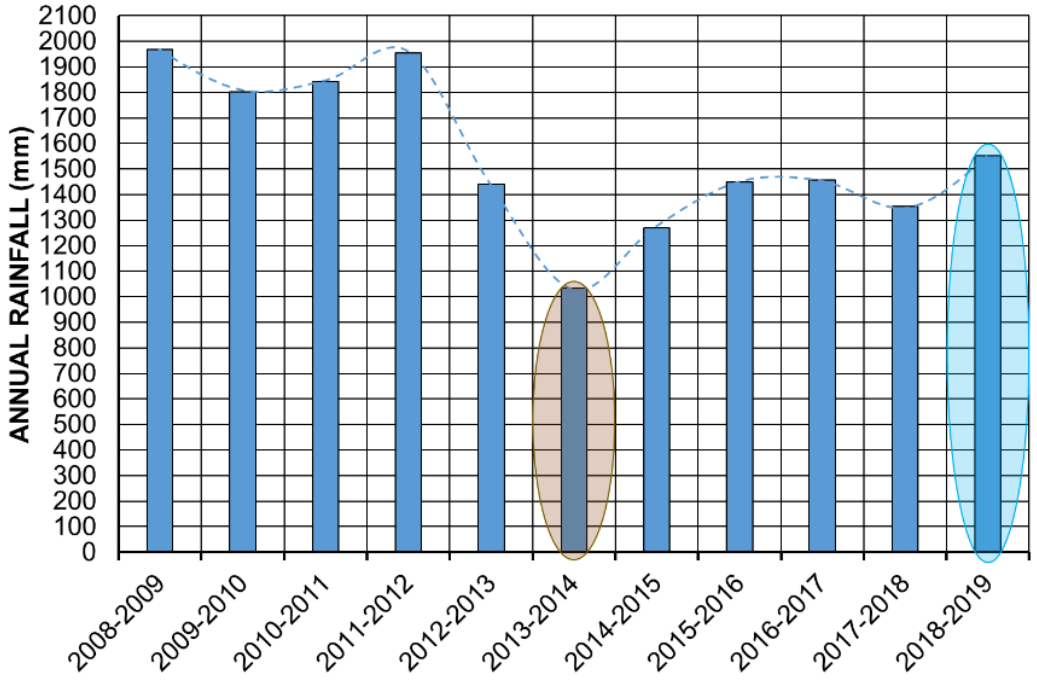

Figure 1: Annual Rainfall for the 10-year Period from 2008-2009 to 2018-2019 at the INMET Ibirité Weather Station

Figure 2 shows the cumulative daily rainfalls from August 1 to January 25 (i.e., including the wet season) for each of the last 10 years at the INMET Ibirité weather station. In the early part of the 2018-2019 wet season, this station showed that the area had close to the wettest cumulative rainfall in the 10-year period.

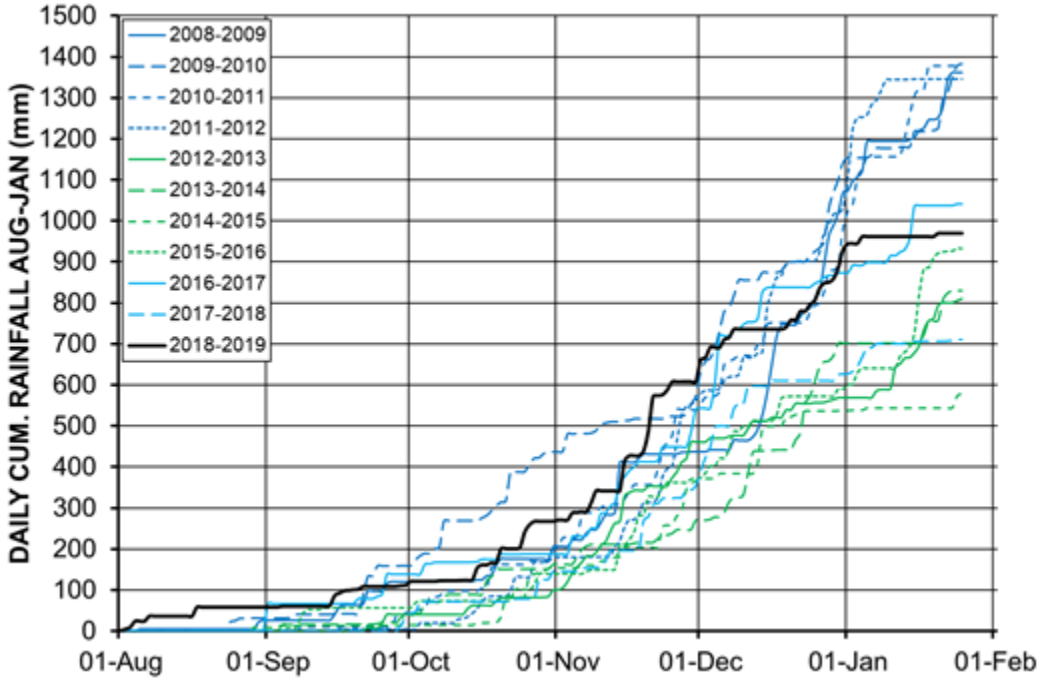

Figure 2: Wet Season Rainfall from August 1 to January 25 for Each Year of the 10-year Period from 2008-2009 to 2018-2019 at the INMET Ibirité Weather Station

Figure 3 highlights the periods of intense rainfall during the 2018-2019 wet season leading up to the failure.

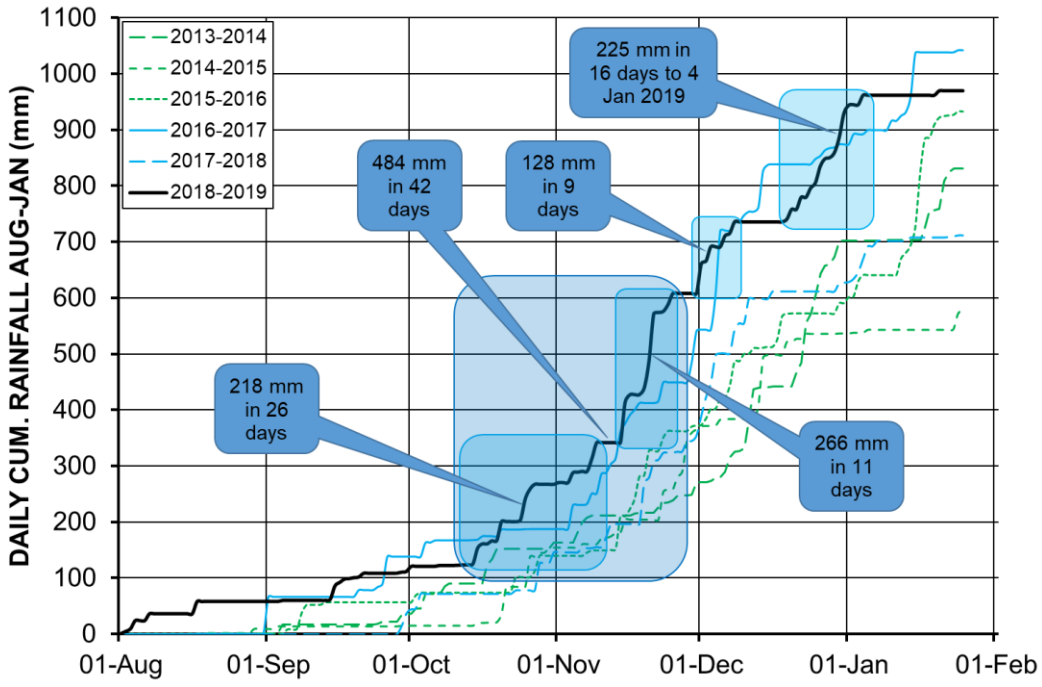

Figure 3: Wet Season Rainfall from August 1, 2018, to January 25, 2019, for INMET Ibirité Weather Station with Highlighted Intense Periods

In addition to a review of the INMET Ibirité weather station, data from F11 and F18 were considered. Figure 4 compares the cumulative daily rainfalls for the period from August 1, 2018, to January 25, 2019, for the INMET Ibirité weather station and for the F11 and F18 automated rain gauges, and shows they are broadly comparable and are all suitable for use in the seepage analyses.

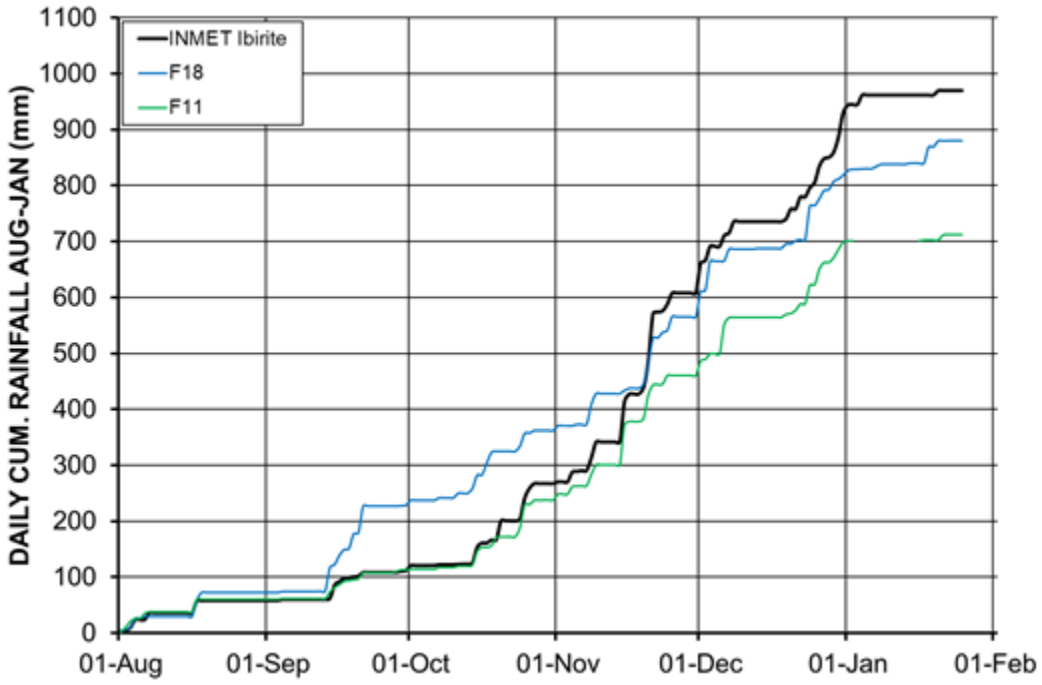

Figure 4: Comparison of Wet Season Rainfall from August 1, 2018, to January 25, 2019, for the INMET Ibirité Weather Station and for the F11 and F18 Automated Rain Gauges

3.2 Preliminary Modeling to Calculate the Net Infiltration of Rainfall

Using the 1D coupled soil-atmospheric computer model SoilCover,[1] a preliminary simulation was performed to establish an estimate of the percentage of rainfall that would infiltrate Dam I. A one-year simulation was conducted using data from the INMET Ibirité weather station for the 12-month period from January to December 2018 to include both the wet and dry seasons. A saturated coefficient of permeability (or hydraulic conductivity, k_{sat}) equal to $5x10^{-6}$ meters per second (m/s) was selected for the surface of the tailings on the basis of Guelph permeameter measurements conducted on site (Appendix E) and the soil-water characteristic curves (SWCC) obtained from laboratory tests (Appendix E, Annex 7).

The calculated net infiltration rate on the dam was approximately 50% of the annual rainfall. The calculated net infiltration rate over the slimes in the pond area is estimated to have been smaller at around 20%, based on a saturated vertical k_{sat} equal to $1x10^{-8}$ m/s for the slimes. In addition, most

[1] GeoAnalysis. (2000). *SoilCover software user's manual*. Saskatoon, SK: University of Saskatchewan.

of the rainfall and associated net infiltration is concentrated within the relatively short wet season of four to five months.

3.3 Detailed Modeling to Calculate Net Infiltration of Rainfall

More comprehensive modeling of climate flux boundary conditions was performed with SVFLUX™. The results of this modeling were used to specify the net infiltration rate of rainfall for the seepage models. Calculations were performed to determine both potential evaporation (PE) and actual evaporation (AE) at a partly saturated ground surface. The Fredlund-Wilson-Penman (2000)[2] calculation method of AE was employed, which requires the input of: (i) rainfall; (ii) temperature; (iii) relative humidity; (iv) windspeed; and (v) net radiation.

For rainfall, data from F18 were used, with supplemental data from F11. Relevant data from F18 spanned from March 2017 through January 2019. Data from F11 covered the period from January 2016 through January 2019. To extend the F18 data back to the start of 2016, a two-step method was used. To start, the first two months of data (January 1 to March 1) from 2018 and 2019 were averaged to estimate the rainfall data for the early portion of 2017. Then, the F11 data from 2016 were utilized to supplement the F18 data. The average annual rainfall determined from complete rainfall years from F18 data, supplemented by F11 data, was 1400 millimeters per year (mm/year).

Detailed climatic information, such as relative humidity and net radiation, was not available from F18 or F11. Hence, the INMET weather station was utilized to supplement information unavailable from F18 and F11, to provide a complete climatic dataset required for the seepage model.

A 1D seepage saturated/unsaturated model was established to calculate the net infiltration due to rainfall into the tailings. The location of the extracted 1D model is shown in Figure 5.

[2] Wilson, G.W., Fredlund, D.G., & Barbour, S.L. (1997). The effect of soil suction on evaporative fluxes from soil surfaces, *The Canadian Geotechnical Journal*, *34*(4), 145-155; Fredlund, M.D., Tran, D., & Fredlund, D.G. (2016). Methodologies for the calculation of actual evaporation in geotechnical engineering, *ASCE International Journal of Geomechanics*, *16*(6).

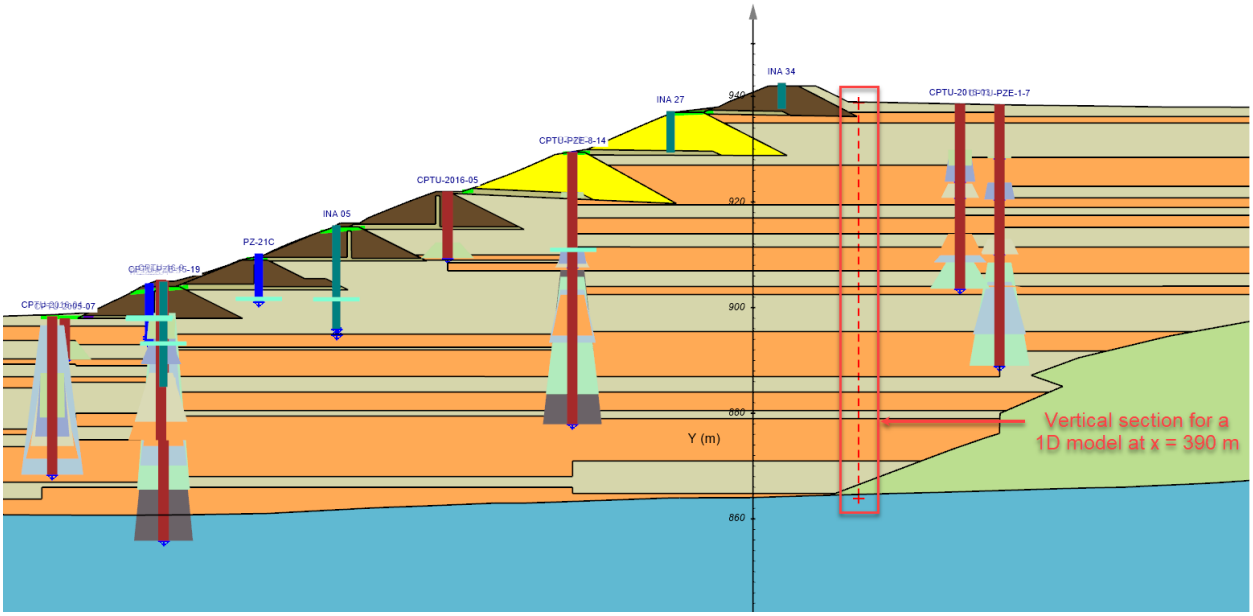

Figure 5: Location of 1D Infiltration Profile Model in 2D Cross-section 2-2

The 1D model incorporated a detailed Fredlund-Wilson-Penman (2000) boundary condition, as discussed above. The Thornthwaite method[3] was utilized to determine PE, and an annual PE of 945 mm at the site was calculated.

The base of the 1D model was set close to the foundation in the 2D model. The bottom boundary condition was set as the head calculated in the 2D model. Details on the 2D model are provided later. The 1D model was run for five years with 2017 climatic data to provide a reasonable initial condition. The model was subsequently run with climatic weather station data from 2018 until failure in January 2019, using the initial conditions obtained from the five-year simulation of 2017 climatic data. Vertical permeability was set at one-fifth of horizontal permeability, and the Fredlund, Xing, and Huang method[4] was used to calculate unsaturated permeability curves.

The rainfall, evaporation, and recharge cumulative effects show that the infiltration in the system is approximately 50%. The net infiltration of rainfall rate of 50% was used as surface flux

[3] Thornthwaite, C.W. (1948). An approach toward a rational classification of climate. *Geographical Review*, *38*, 55-94.

[4] Fredlund, D. G., Xing, A., & Huang, S. (1994). Predicting the permeability function for unsaturated soils using the soil-water characteristic curve. *Canadian Geotechnical Journal*, *31*(4), 533-546.

boundary conditions in the saturated/unsaturated seepage models described in the following sections.

4 SEEPAGE MODELING AND CALIBRATION

Seepage modeling was carried out initially in 2D followed by 3D simulations. The following sections describe the conceptual model used, the review of available data, and model calibration.

Construction of the dam began in 1976, and the final raise was completed in 2013. Tailings deposition ended in 2016. Piezometric data are available from 1996 up to the failure in January 2019. The focus of the seepage modeling was for the three-year period prior to failure, starting in January 2016, during the period of time when no further tailings deposition was performed.

This seepage model and calibration process provide representative flow conditions in the tailings, which will then allow:

- The prediction of steady-state flow conditions at each stage of construction; and
- The prediction of transient flow conditions leading up to the January 2019 failure.

4.1 Conceptual Model

The conceptual model for the site is illustrated schematically in Figure 6. The various potential inflows and outflows to the tailings dam are shown. The runoff from the beach and from the drainage basin is addressed through maintenance of the water levels in the pond. Evaporation was determined through calculations using the Thornthwaite method. Drainage from surface drains is reported in the field measurements (discussed in Appendix C). These drains are assumed to be connected to blanket drains, as discussed in Section 4.5.5. The subsequent modeling exercise quantified the effect of the various contributors to the mass balance of the system.

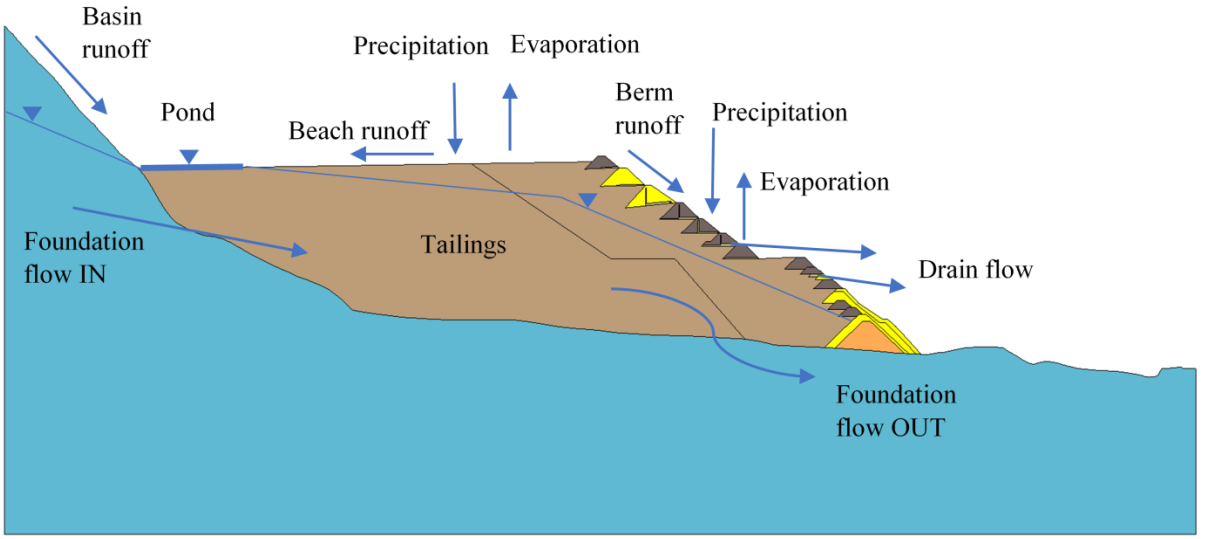

Figure 6: Site Conceptual Model

4.2 Review of Available Data

A critical component in the seepage and calibration modeling was to match the model to all known field measurements, which included: (i) piezometers; (ii) water level indicators (INAs); (iii) cone penetration test (CPTu) pore water pressure measurements; and (iv) flow rates from drains located on the downstream face of the dam.

In building the seepage model, some parameters are known based on available data and some are determined through the calibration process. Table 1 summarizes the seepage parameters and the methodology used to determine the parameters.

Table 1: Sources of the Model Parameters

Area	**Parameter**	**Source**
Geometry	Berm locations	Appendix A
	Tailings layers	Appendix F
	Piezometer/INA locations and measurements	Appendix C
	CPTu locations and measurements	Appendix B

	Blanket/chimney drain locations	Appendix A and calibration
	Assumed surface expression of blanket drains	Appendix C
	Deep horizontal drains (DHPs)	Appendix C
Material properties	Saturated coefficient of permeability	CPTu testing (Appendix B)
	Foundation coefficient of permeability	Estimated
	Compacted tailings coefficient of permeability	Estimated
	Unsaturated coefficient of permeability	Estimated
	Soil-water characteristic curve (SWCC)	Appendix E, Annex 7
	Anisotropy	Estimated and calibrated
Boundary conditions	Upstream	Sensitivity analysis
	Downstream below dam	Ground surface
	Downstream berms	Combined % of rainfall and drainage
	Tailings – pond	Pond area and head
	Tailings – beach	% of rainfall
	Climate – rainfall	Appendix C
	Climate – evaporation	Appendix C, with additional calculations
	Infiltration/recharge	Calculated and calibrated

Calibration of the seepage model required a review of existing historical data as well as an inclusion of data from post-failure field and laboratory tests (see Appendices B, C, and E). The

focus of the calibration process is on the three years prior to the failure during which tailings deposition had stopped.

The methodology for calibration of the seepage model was a manual sensitivity analysis involving over 150 models and was comprised of the following steps:

1. **Infiltration calibration:** The climate rainfall data were known for the period 2016-2019 from F18 and F11. What is unknown is the amount of net rainfall infiltration or recharge resulting from the net effect of rainfall, runoff, and evaporation. Models were run with net infiltration estimates of 30%, 50%, and 70% of rainfall, and the resulting water pressures were compared to measurements of piezometers and INAs. The calibration was first run with homogeneous tailings and later with heterogeneous layered tailings (coarse/fine/slimes).

2. **CPTu calibration:** The homogeneous and heterogeneous tailings models were calibrated to the CPTu data. The CPTu pore water pressure readings were noted to be approximately 50% of hydrostatic. The foundation coefficient of permeability as well as the anisotropy of the tailings materials were adjusted to match CPTu readings.

3. **Drains:** Blanket and chimney drains (i.e., L-shaped drains) as well as deep horizontal drains (DHPs) were implemented in the model, and calibration to drainage flows, piezometer, INA, and CPTu data were updated.

4. **2D/3D:** The 2D models were utilized in the calibration process first to reduce model times. After 2D calibration was achieved, 3D models were examined.

The above process allowed determination of the remaining few model parameters by matching field data recorded at the site. Specific key components and results of the seepage modeling and calibration program are provided in the following sections and subsections.

4.3 2D Geometry

The geometry was constructed as a 3D model from which 2D cross-sections were then extracted. Seepage modeling was initially performed on the 2D cross-sections. Details on model development are provided in Appendix F.

The seepage model for Dam I was constructed as a series of 10 raises (15 stages) shown in Figure 7. The assumed location of the vertical and/or blanket drains detailed in the design documents can be seen in Figure 7 on raises 4-10. Results of the calibration of the seepage model corroborated

the understanding that drains recommended in design documents for the Second Raising were likely installed (Appendix A). These drains are discussed in Section 4.5.5.

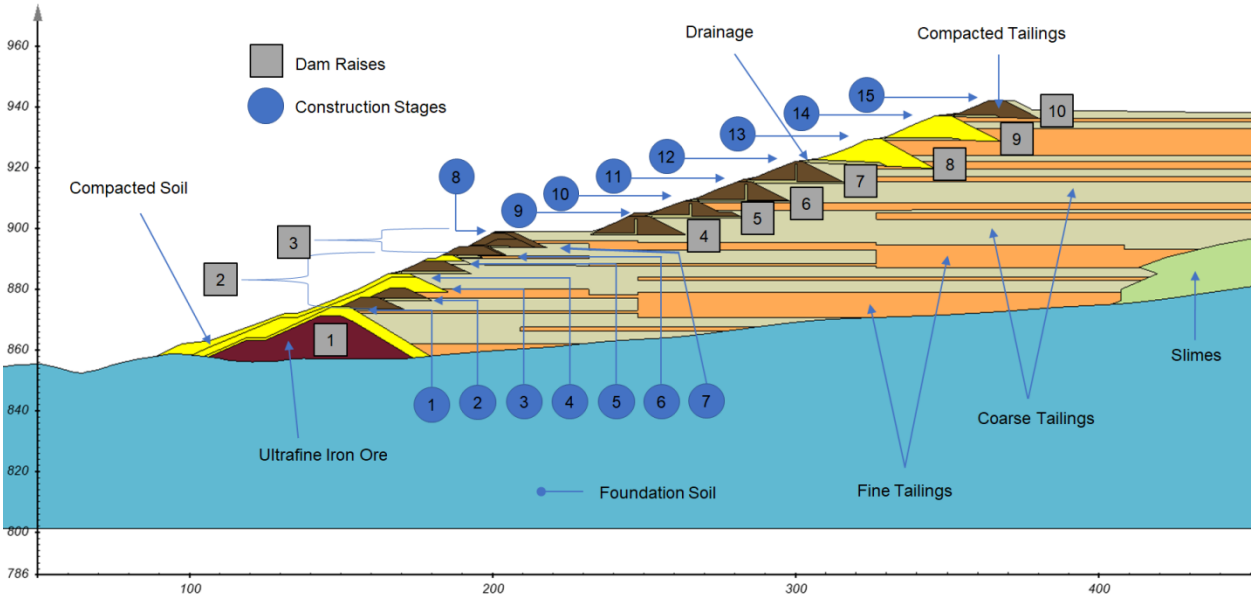

Figure 7: Raises and Stages of Dam I[5]

4.4 Material Properties

Material properties for the seepage modeling were assembled using the parameters provided in Appendix E, as well as from historical reports described in Appendix A.

Historical reports provided a basis for porosities, grain-size distributions, and saturated coefficient of permeabilities. SWCCs[6] and unsaturated permeability curves were also required for the seepage modeling process. A methodology was adopted initially to calculate the unsaturated permeabilities of the coarse/fine/slimes tailings materials based on grain-size distribution curves.

5 See generally Appendices A and F.
6 Appendix E, Annex 7.

4.4.1 Porosity and Specific Gravity

The porosity and specific gravity for all materials presented in Table 2 were based on historical reports and laboratory testing of materials collected post-failure (Appendices B and E, respectively).

Table 2: Porosity and Specific Gravity of Material Used in Seepage Simulations

Material	Porosity	Specific Gravity
Foundation soil	0.31	2.75
Blanket drain	0.40	4.53
Ultrafine iron ore	0.30	4.53
Coarse tailings	0.50	4.53
Fine tailings	0.59	4.63
Slimes	0.49	4.00
Residual soil	0.31	2.75

4.4.2 Saturated Coefficient of Permeabilities

Saturated coefficient of permeabilities, (k_{sat}) were selected based on the historical data and testing. The saturated coefficient of permeabilities adopted are shown in Table 3. The tailings were split into layers to delineate the coarse and fine tailings, and slimes zones. The coarse, fine, and slimes geometric delineation were provided along with the 2D and 3D geometries for the seepage modeling, which are detailed in Appendix F.

The value of k_{sat} for the compacted tailings in the berms was listed in historical reports as the same as fine tailings and was assumed to be one order of magnitude lower than the coarse tailings due to the fact that the compaction process will increase the density and reduce the coefficient of permeability.

Table 3: Saturated Permeabilities Utilized for the Calibration Study

Material	k_{sat} (m/s)	Comments
Fines tailings	1.0E-7	Selected by the Panel based on field testing (Appendix B)
Coarse tailings	5.0E-6	Selected by the Panel based on a field test range between 1.0E-5 to 1.0E-6 (Appendix B)
Compacted tailings	5.0E-7	Selected by the Panel based on field testing and assumed one order of magnitude less than coarse tailings
Slimes	1.0E-8	Selected by the Panel based on field testing (Appendix B)
Ultra-fine iron ore	1.2E-6	Selected based on historical reports[7]
Compacted soil (Laterite)	1.2E-9	Selected based on historical reports[8]
Foundation soil	9.2E-8	Average value using CPTu (Appendix B)
Drainage soil	1.0E-4	Selected based on historical reports[9]

[7] Periodic Review of Dam Safety of the Córrego Feijão Mine – Dam I Technical Report (TÜV SÜD 2018) ("2018 TÜV SÜD Periodic Safety Review").
[8] 2018 TÜV SÜD Periodic Safety Review.
[9] 2018 TÜV SÜD Periodic Safety Review.

Although there may have been compaction of the coarse/fine/slimes tailings due to loading effects of tailings deposited in subsequent layers, it was considered that the variation in coefficient of permeability with depth in the tailings is reasonably small and was not evaluated further.

4.4.3 Unsaturated Permeabilities

The following methodology was adopted to calculate unsaturated hydraulic parameters for the coarse/fine/slimes tailings.

1. Curve fitting the grain-size distributions using the Fredlund and Xing (1994) method.[10]
2. Calculate SWCCs for each grain-size curve using the Fredlund and Wilson (1997)[11] method.
3. Calculate an unsaturated permeability curve using the Fredlund, Xing, and Huang (1994) method.
4. Determine average SWCC and average unsaturated permeability curve for each tailings type.
5. Compare calculated SWCCs and unsaturated permeability curves with measured SWCCs and unsaturated permeability curves based on laboratory tests.

Measured grain-size distributions were used to calculate preliminary SWCC and unsaturated permeability curves for coarse/fine/slimes tailings as well as the natural foundation soils. Figures 8, 11, 14, and 17 show the measured grain-size distribution curves used. Figures 9, 10, 12, 13, 15,16, 18, and 19 show the calculated and measured SWCC, and unsaturated permeability curves.

[10] Fredlund, D. G., & Xing, A. (1994). Equations for the soil-water characteristic curve. *Canadian Geotechnical Journal*, *31*(4), 521-532.

[11] Fredlund, M.D., Fredlund, D.G., & Wilson, G.W. (1997). Prediction of the soil-water characteristic curve from grain-size distribution and volume-mass properties. Proceedings from NONSAT '97: *The 3rd Brazilian Symposium on Unsaturated Soils*, (S.W. Hong, T. de Campos, & E.A. Vargas, Eds.), Rio de Janeiro: Freitas Editora.

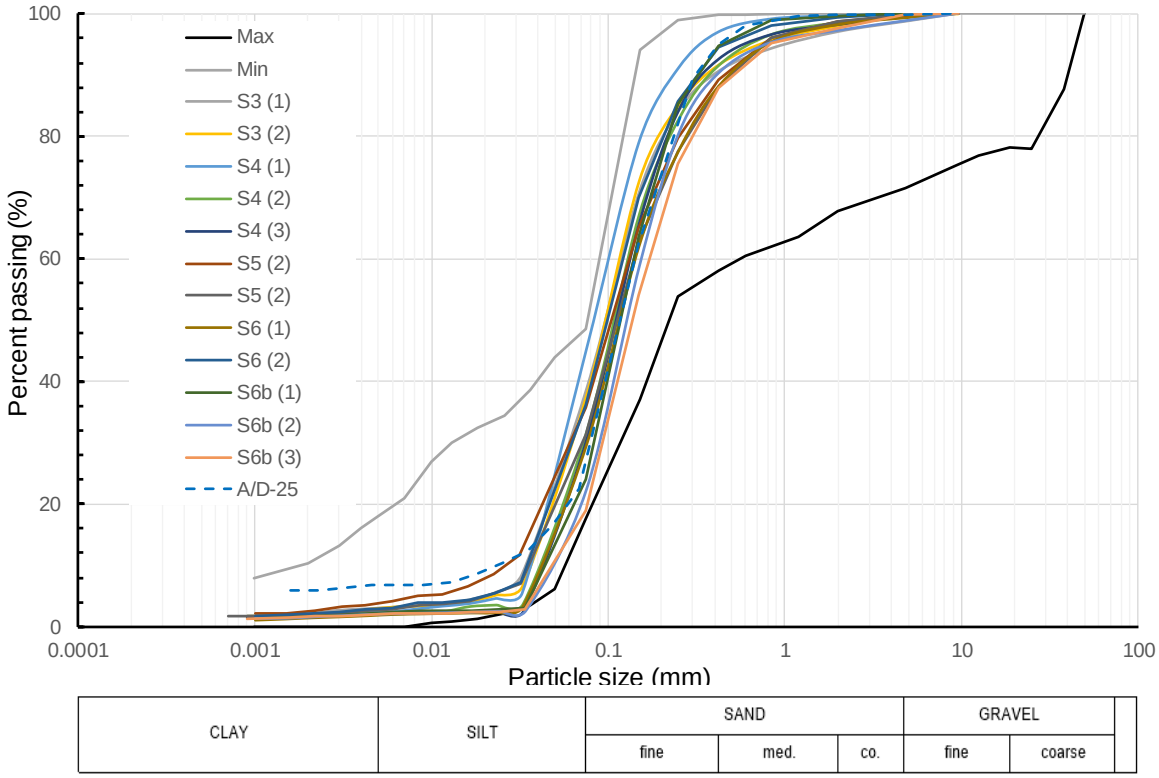

Figure 8: Grain-size Distribution of Coarse Tailings and the Selected Grain Size (A/D-25) to Estimate the SWCC

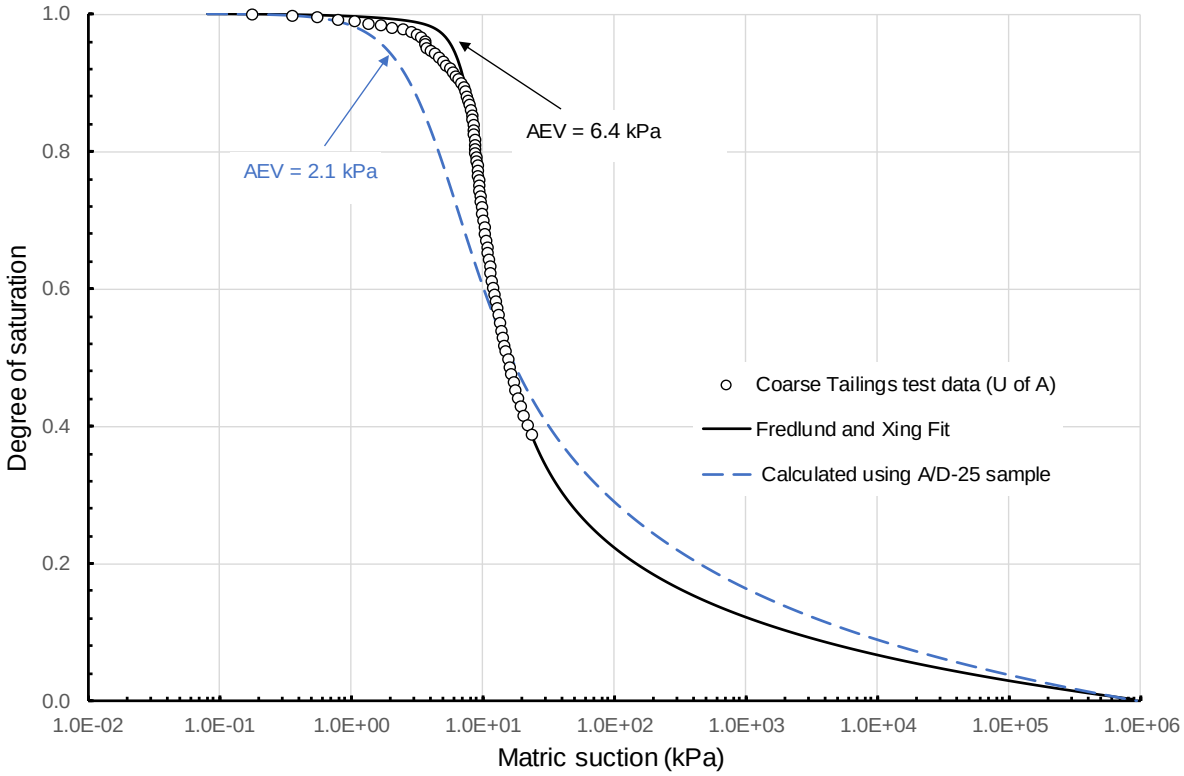

Figure 9: Calculated and Measured SWCC Used for Coarse Tailings

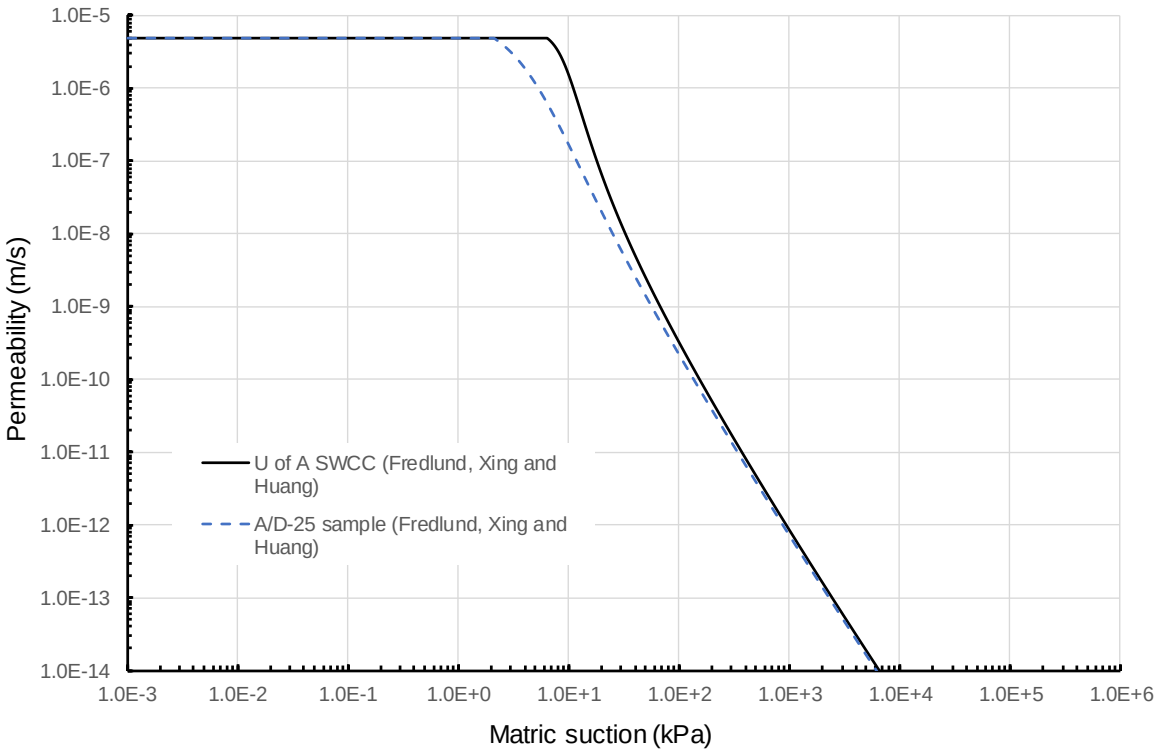

Figure 10: Unsaturated Permeability Curves for Coarse Tailings

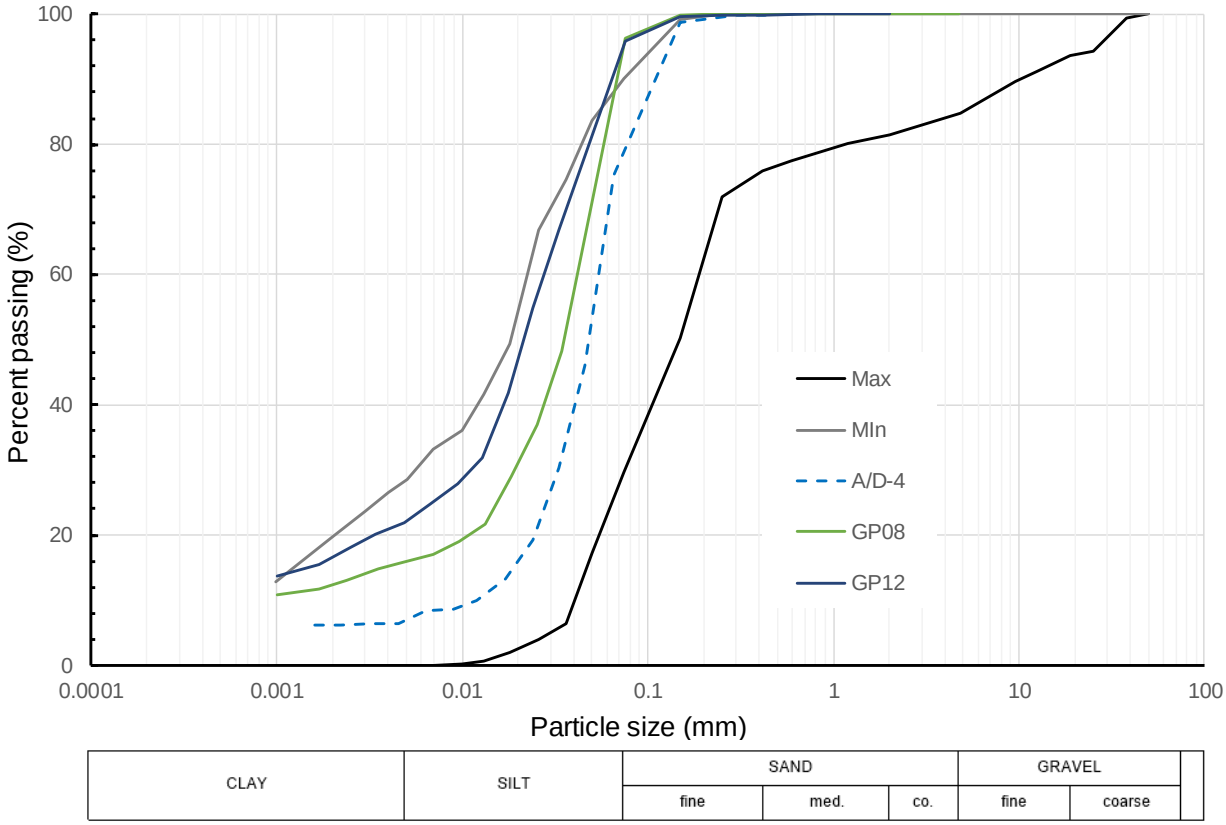

Figure 11: Grain-size Distribution of Fine Tailings and the Selected Grain Size (A/D-4) to Estimate SWCC

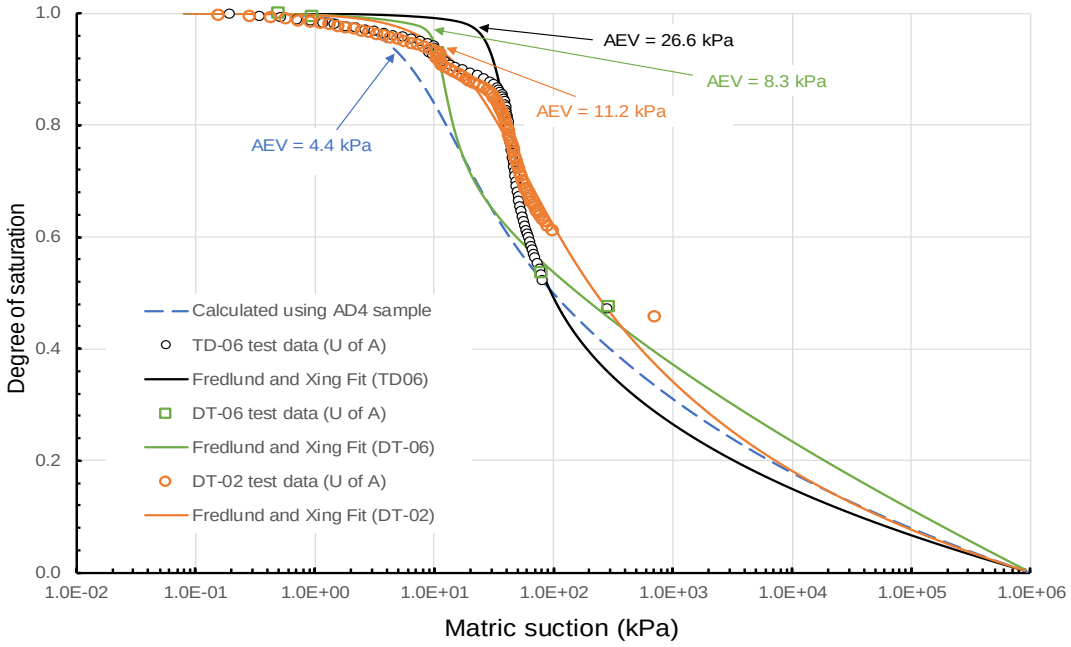

Figure 12: Calculated and Measured SWCC Used for Fine Tailings

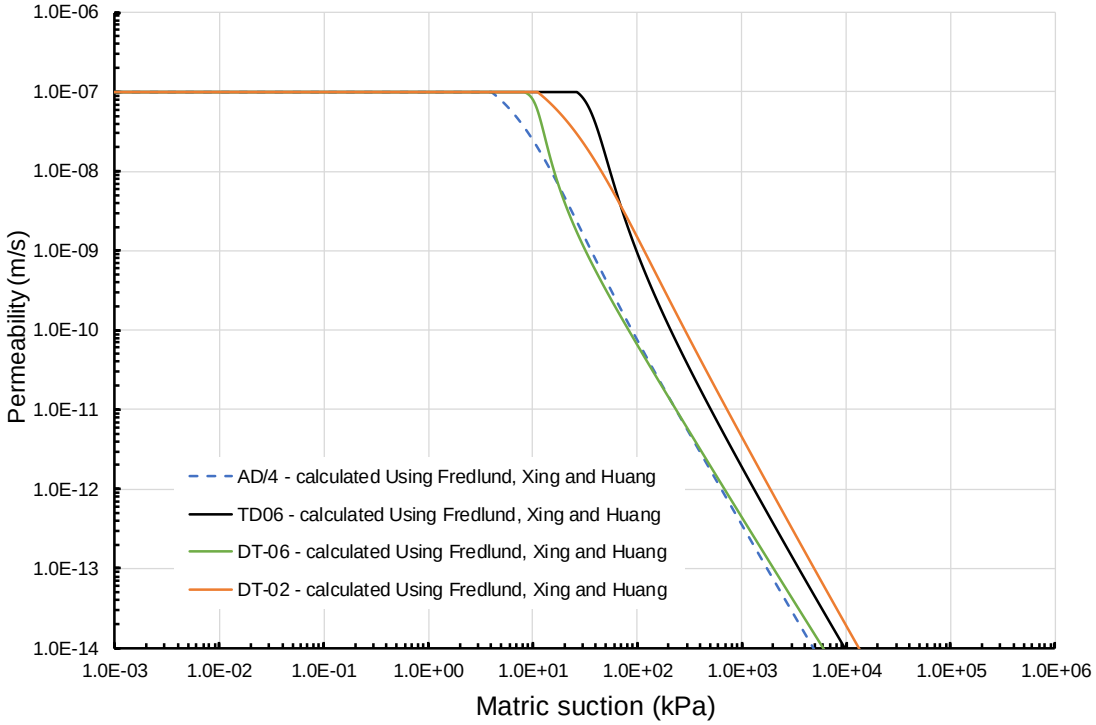

Figure 13: Unsaturated Permeability Curves for Fine Tailings

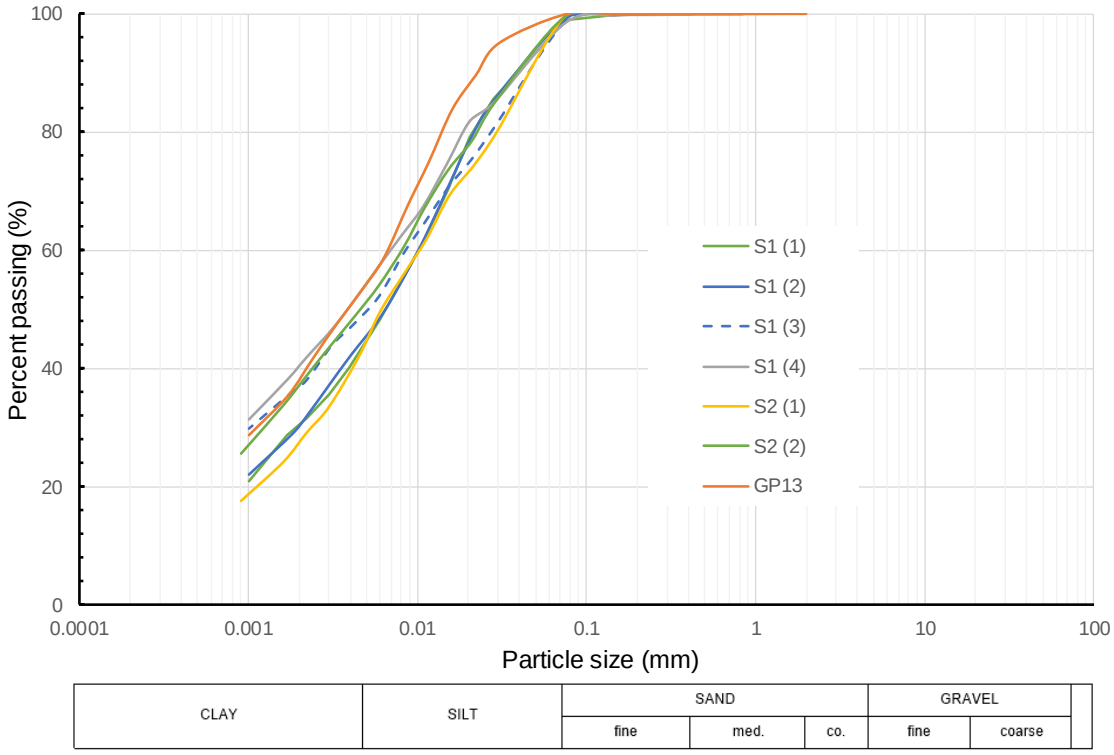

Figure 14: Grain-size Distribution of Slimes and the Selected Grain Size (S1 (3)) to Calculate SWCC

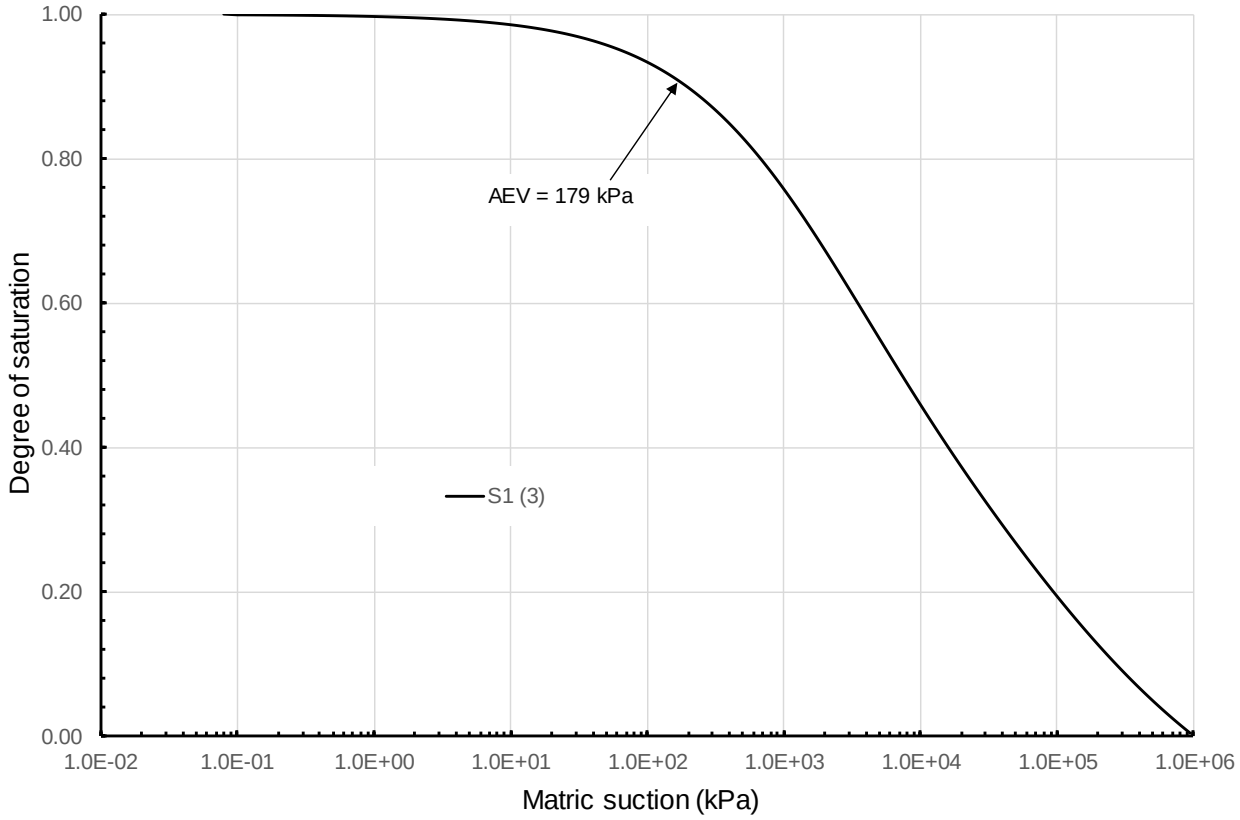

Figure 15: Calculated SWCC Used for Slimes

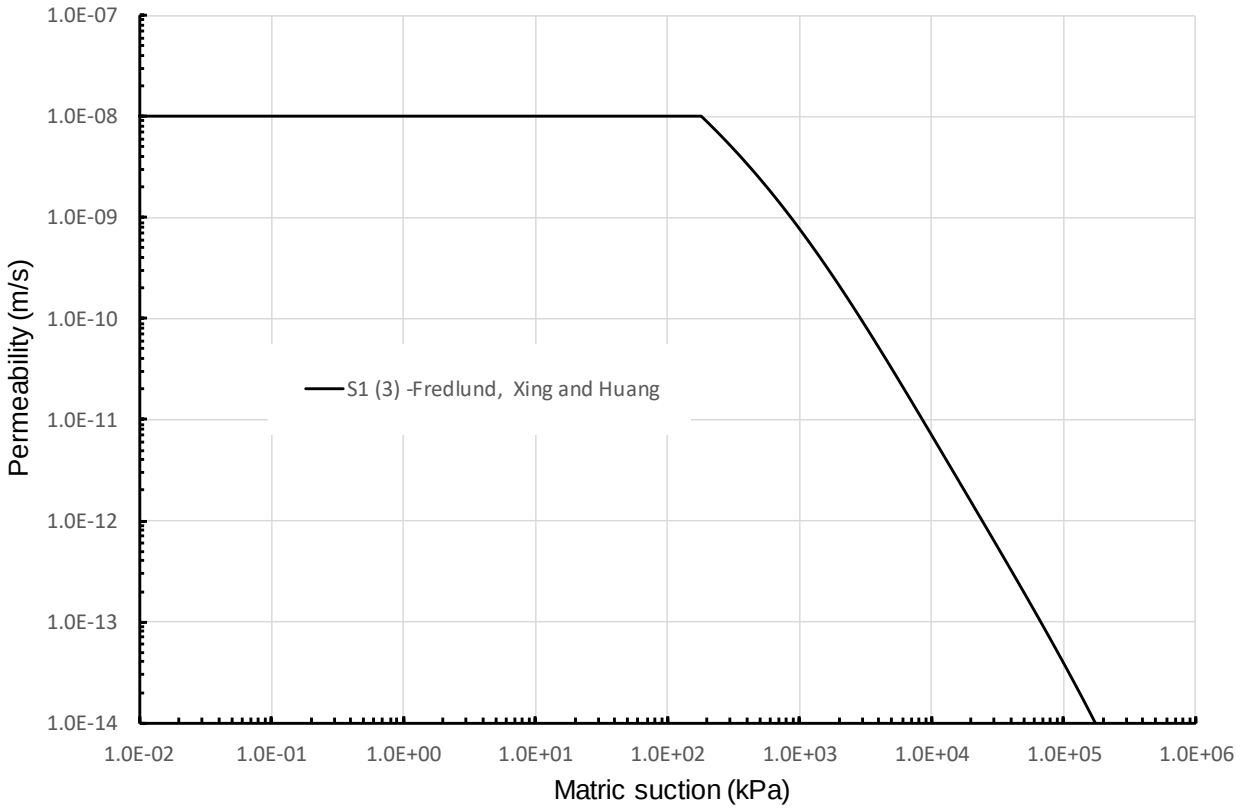

Figure 16: Unsaturated Permeability Curves for Slimes

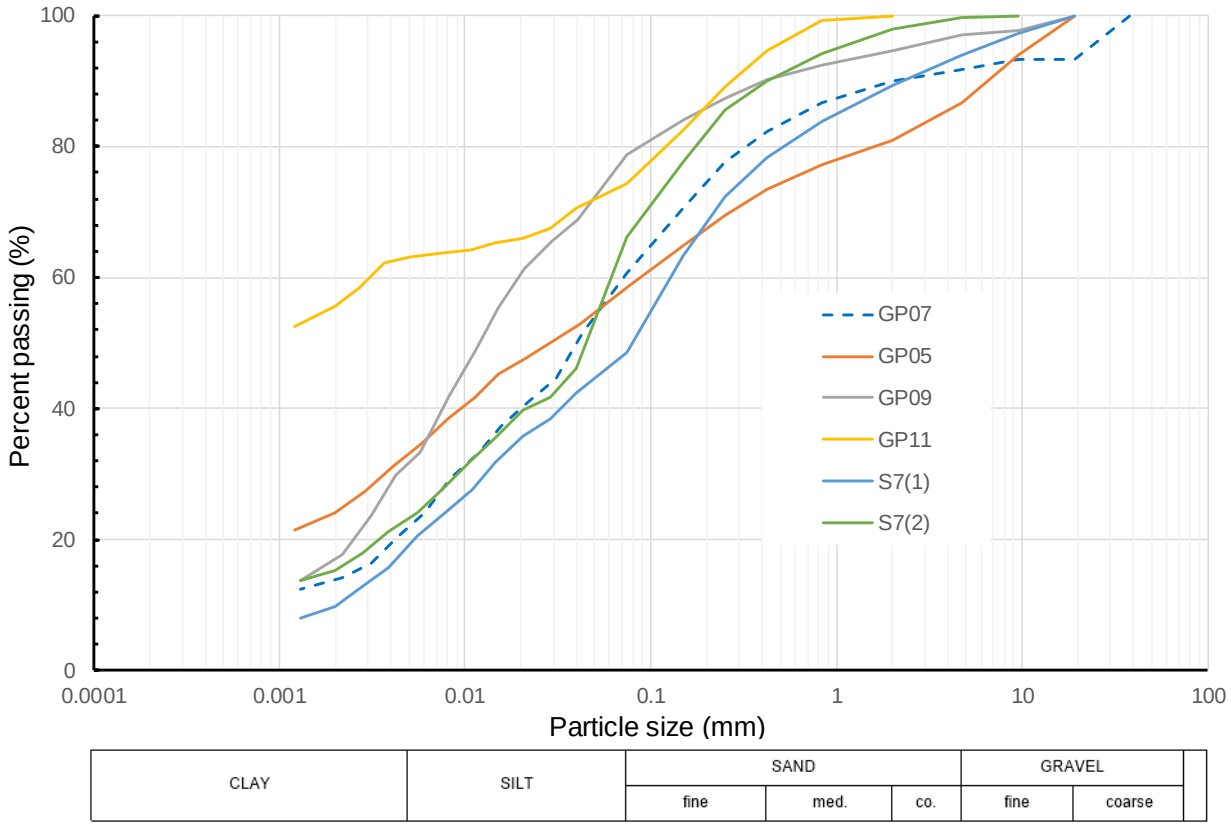

Figure 17: Grain-size Distribution of Natural Foundation (Residual) Soil and the Selected Grain Size (GP07) to Calculate SWCC

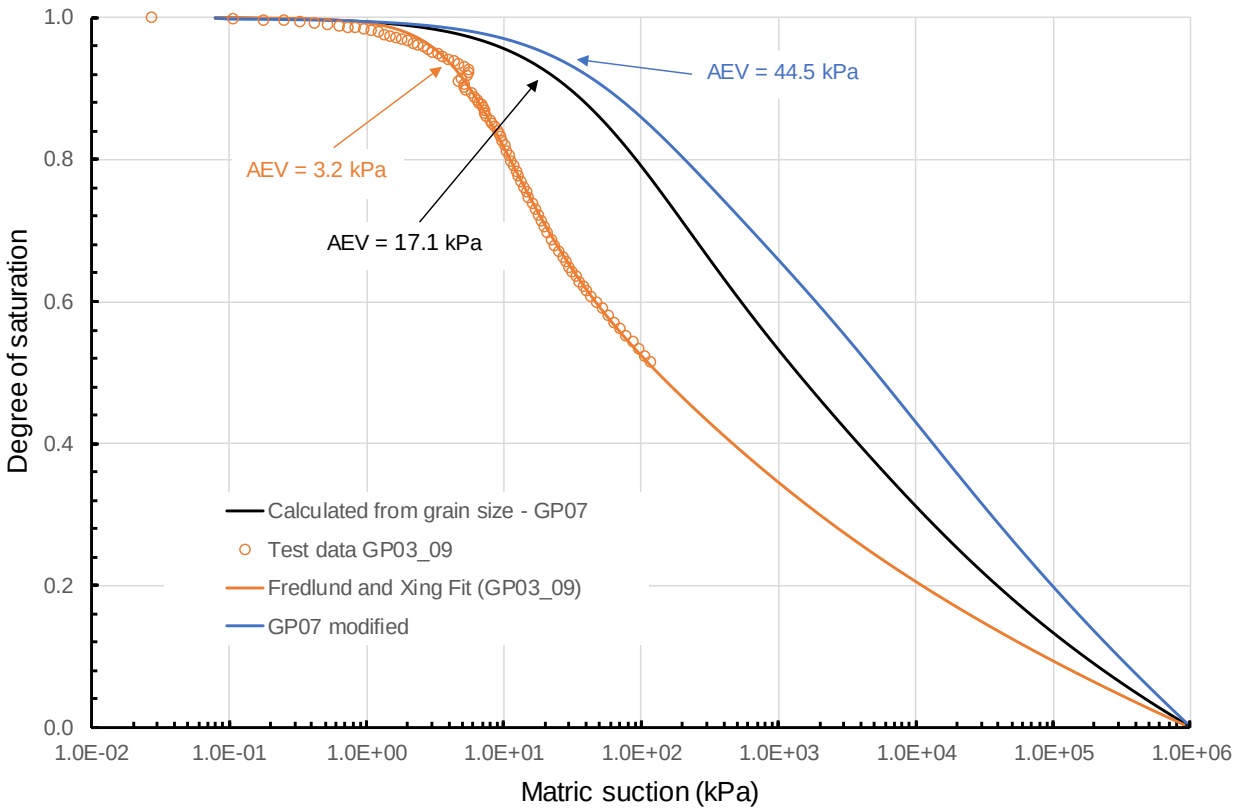

Figure 18: Calculated and Measured SWCC Used for Residual Soil

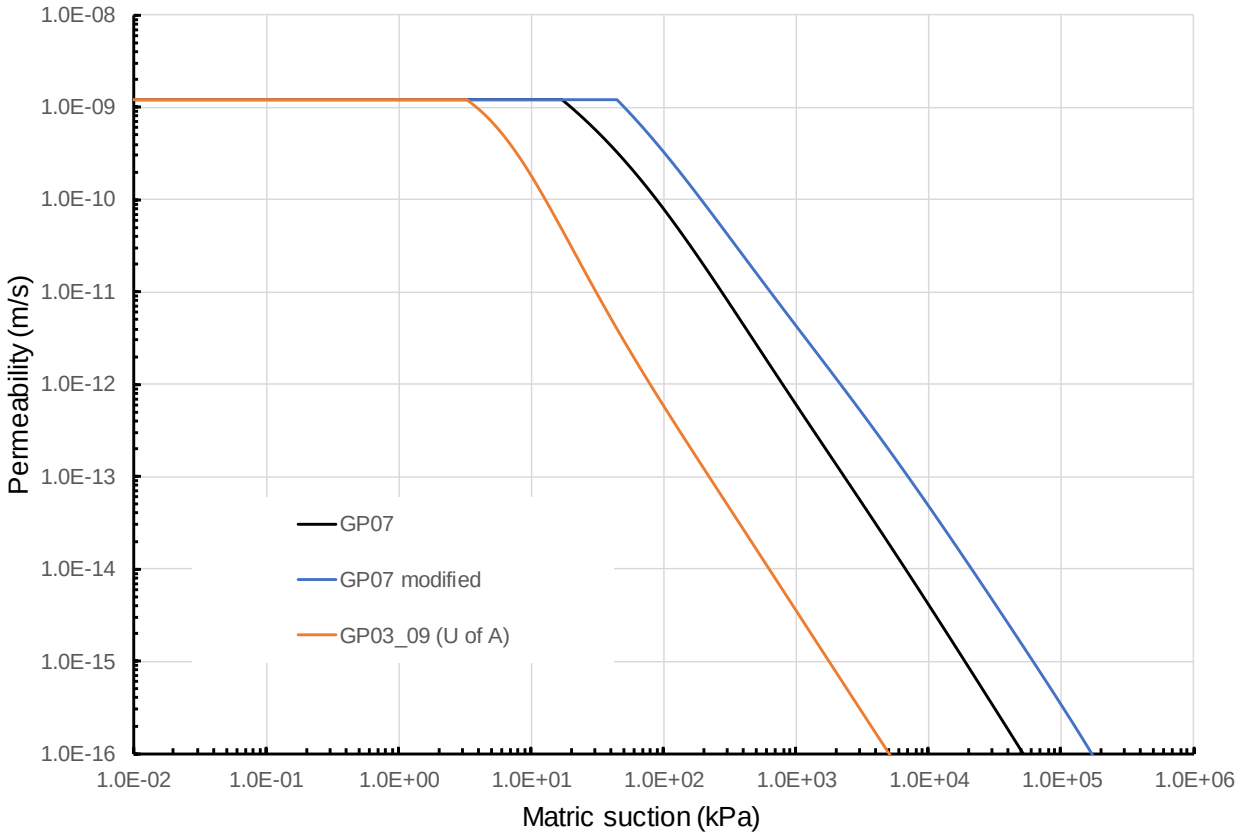

Figure 19: Unsaturated Permeability Curves for Residual Soil

4.5 Boundary Conditions

A key component of the seepage modeling is determining the influence of the boundary conditions on the seepage groundwater flow model. Primary conditions influencing the seepage model are: (i) climate on the beach and berms, including the effects of transpiration; (ii) the pond located on the surface of the tailings; (iii) springs known to exist beneath the dam and observed post-failure; (iv) flows from drains assumed to be connected to blanket drains; (v) flows from DHPs; (vi) any downstream seepage faces; and (vii) foundation flow.

4.5.1 Climate and Infiltration

Details on the influence of climate and infiltration were covered in Section 3.

4.5.2 Surface Hydrology and Upstream Boundaries

Dam I is located in the Córrego do Feijão drainage basin that has an area of 844 hectares (ha) (Appendix A). The area of the tailings impoundment behind the dam is comprised of 250 ha which represents approximately 30% of the entire catchment area. The land behind the tailings impoundment area is heavily vegetated and slopes steeply towards the tailings.

The groundwater seepage model was required to interface with the upstream catchment area and the groundwater flow regime. Interfacing was considered as follows.

4.5.2.1 Surface Runoff

It is possible that surface runoff from the catchment area flowed downhill (if not infiltrated or obstructed by vegetation) to the tailings impoundment. If it reached the tailings, it would be incorporated into the pond. The pond elevation was controlled and measured over time. The net effects of the upstream catchment runoff are considered to be represented by the pond boundary condition in the seepage model.

4.5.2.2 Groundwater Flow Contributions

Subsurface information for the upstream catchment area was not available for inclusion in the groundwater seepage model. A buffer zone extending approximately 5% beyond the dimensions of the tailings impoundment was created around the model where surface elevations were known. High pore-water pressure heads in the surrounding region were assumed. Given the high rainfall in the area, it was considered reasonable to assume that heads in the upstream areas were higher than the tailings. Computer simulations were performed with upstream head boundary conditions between 2-5 m higher than the pond head. The 5 m head difference forced water towards the tailings area but applied rainfall events sometimes caused the upstream catchment area to become saturated. Such upstream heads were considered reasonable in that:

- The flow of water from the catchment area to the tailings is controlled by the foundation material permeability; and

- The contribution of rainfall to the water balance of the tailings has a larger effect than flow from the catchment area.

4.5.3 Pond

The location and size of the pond varied over time, as detailed in Appendix F. The pond is considered a reasonable boundary condition for the seepage model because the approximate pond

elevation was known. It is recognized that the pond is formed through a combination of: (i) rainfall; (ii) beach runoff; (iii) drainage basin runoff; and (iv) tailings consolidation water. The head condition of the pond elevation was applied in the seepage model as a boundary condition, which represents the net effect of all of these processes. It is therefore not necessary to know the precise runoff from the drainage basin, as the ultimate effect of any runoff into the pond will ultimately be controlled through input of the pond water level into the model. The influence of rainfall and runoff is therefore captured in the net effect of the pond boundary condition.

Aerial photographs of the pond at various times are presented in Appendix F. The beach lengths utilized in the seepage modeling of various construction stages is shown in Figure 20.

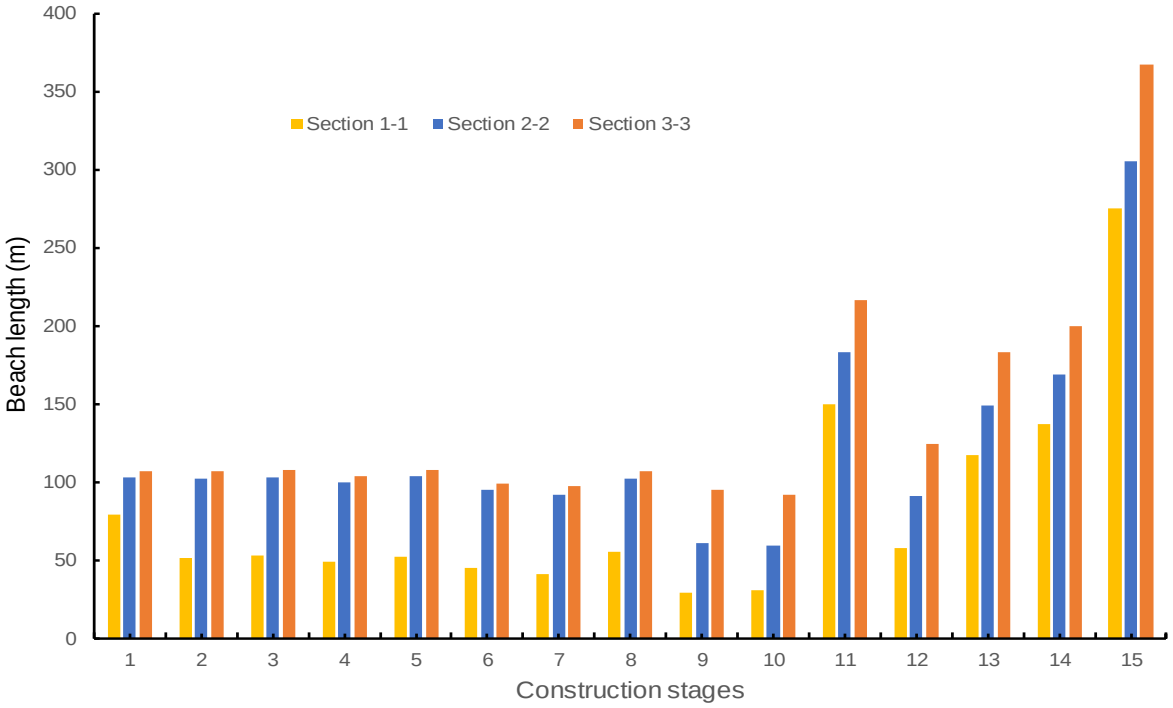

Figure 20: Simulated Beach Lengths at Different Construction Stages

4.5.4 Springs

Springs were observed daylighting at locations identified in Figure 21 and flow rates were measured (Appendix E).

A head of about 2-5 m higher than the average tailings surface was applied to the model boundaries that were set at an average distance of 5% additional distance beyond the dimensions of the tailings impoundment. Such a boundary will allow a net hydraulic gradient towards the tailings in the surrounding foundation material. The coefficient of permeability of the foundation material is less than the coefficient of permeability of the tailings or slimes. It is expected that the water flow into the tailings from the foundation will be small relative to the contribution of the pond and the rainfall to the water balance in the tailings.

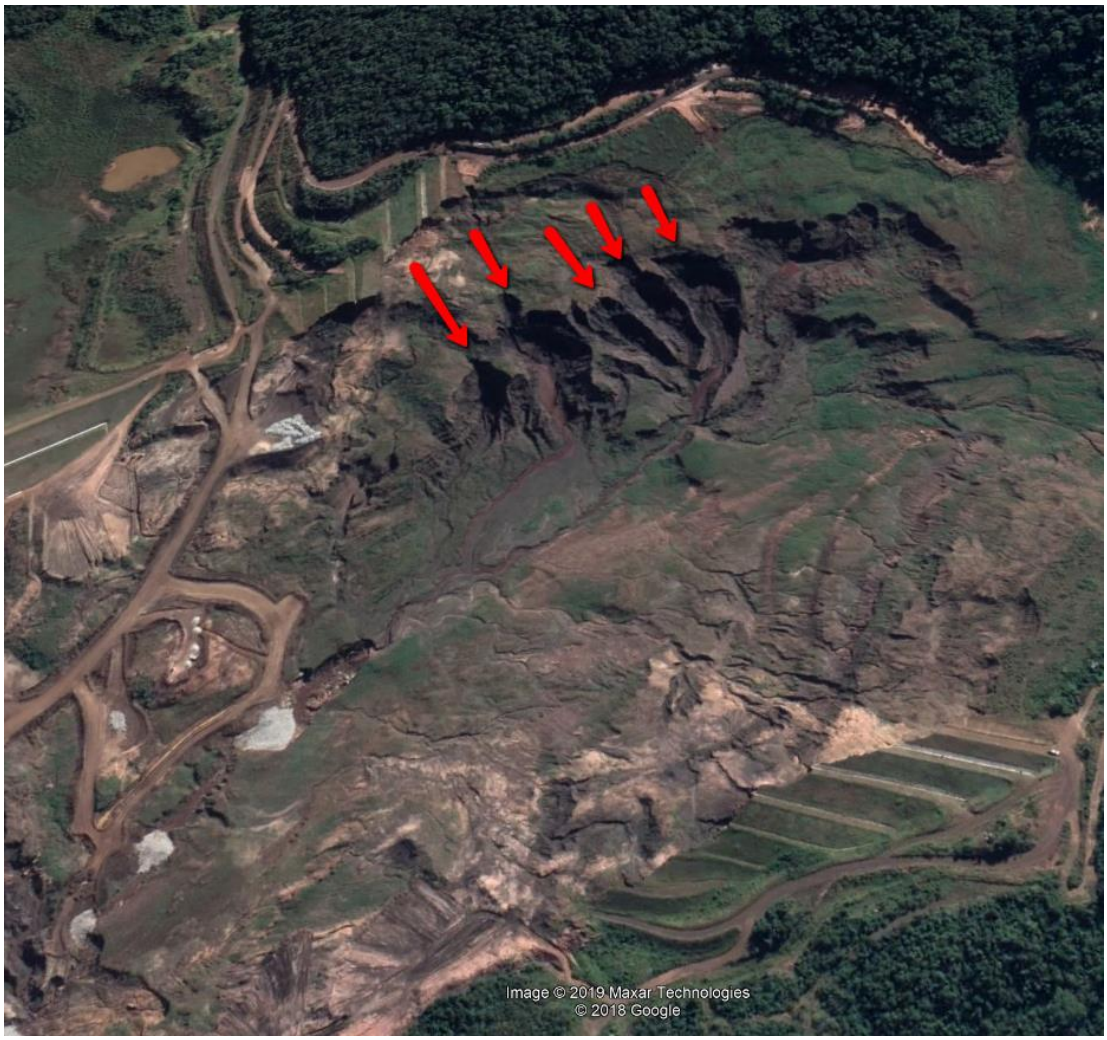

Figure 21: Location of Post-failure Daylighting Springs

4.5.5 Drains

Blanket and chimney drains composed of higher coefficient of permeability coarser material were installed in some of the stages, as described in Section 4.3 and in Appendix A. It is worth noting that the drains were designed to be installed at the base of berms and therefore can be thought of as providing drainage for water that reaches the drains where a positive pore water pressure exists. The blanket drains were conceptualized as draining the water close to the berm on the downstream side of the tailings. Conversely the blanket drains do not reduce pore water pressures in the general tailings mass but only in the berms and the tailings immediately adjacent to the berms. It is therefore possible for a water table to exist relatively close to the berm structures.

Based on design documents described in Appendix A and calibration results discussed in Section 4.3, the blanket drains were assumed to have been installed in the base of the berms from raises 2 through 10, as described in Appendix A. Corresponding chimney drains were installed in Stages 8 through 11. Blanket drains were modeled as being connected to the surface drainage system through surface drainage pipes inserted into the blanket drain material. It is assumed that the drains are connected to internal filter blanket layers. The drains demonstrated intermittent flow (Appendix C). The drains were installed between 1990 and 2000, and monthly measurement of flow is available from April 1, 1996. The last measurement of flow was on December 13, 2018. The locations of the drains and the data from 2014 up to the failure are shown in Appendix C. The majority of flows range between 0.5 and 4 m^3/hr.

The location of the blanket and chimney drains as assumed in the model can be seen in Figure 22.

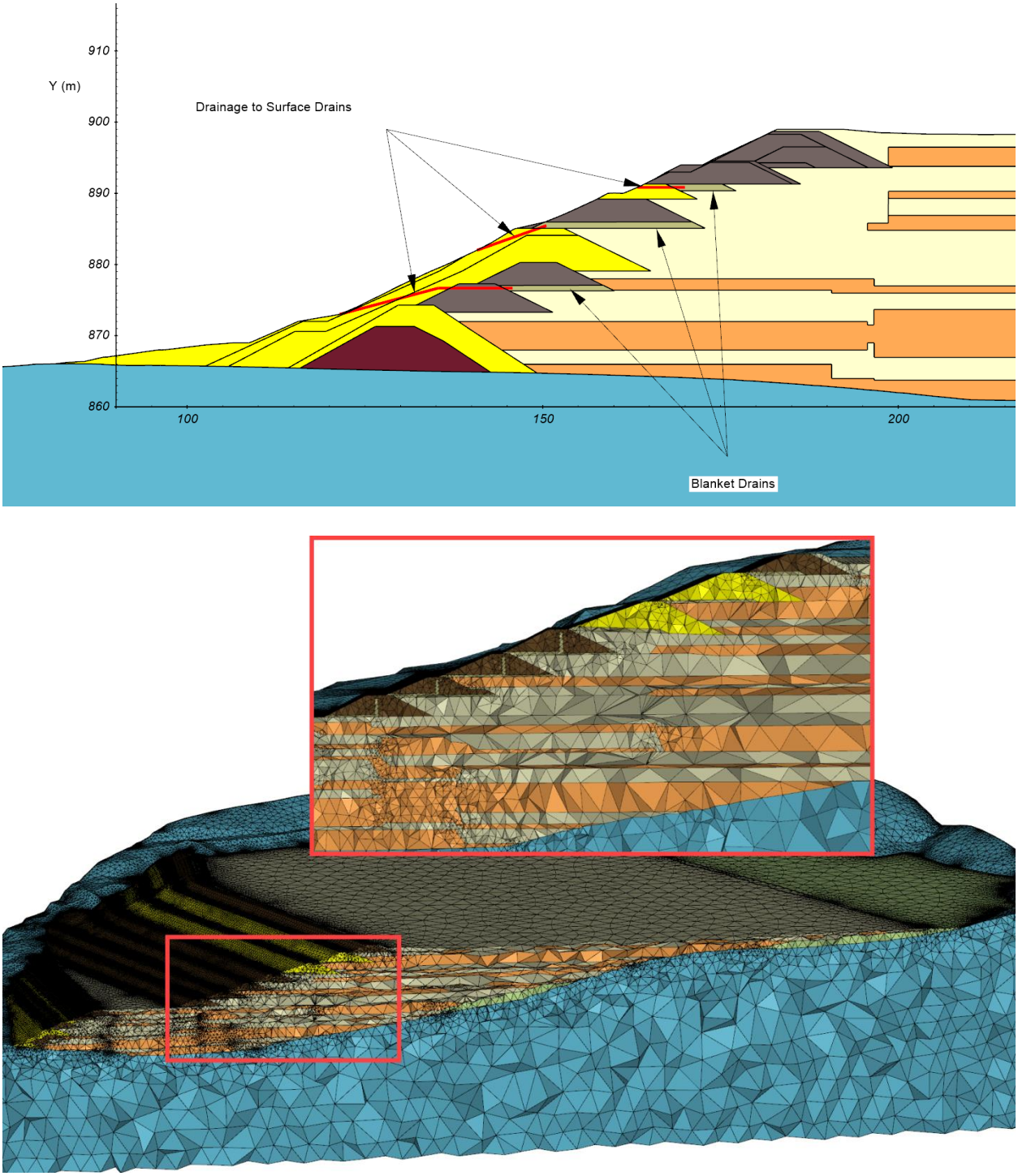

Figure 22: Assumed Location of the Drains and Details

4.5.6 Deep Horizontal Drains

DHPs were installed in 2018 and measurements were taken between May and December 2018. Details regarding measurement and installation are set out in Appendix C.

4.5.7 Downstream Seepage Faces

Sporadic references of damp/wet areas on the downstream faces of the dam are encountered in the historical documents (Appendix A) and was observed in the image analysis (Appendix D). It is difficult to quantify if the wetness is caused by a daylighting of the water table or saturation from rainfall events. Both types of downstream surface wetness were observed in the numerical model.

4.6 Water Pressure Field Measurements

4.6.1 Piezometers and Water Level Indicators

Data was available from 163 piezometers and INAs (Appendix C). The location of the piezometers and INAs and their associated data can be found in Appendix C. The readings started in 1996, but not all were continuous. The majority of readings were manual until 2019 when 49 of the piezometers were automated. Some of the piezometers and INAs were not able to be used in the calibration because of various issues with the data. In some cases, installation or location data were unreliable, as described in more detail in Appendix C, and therefore the entire instrument was not used. In other instances, certain individual data points were not used in the calibration because they indicated sizeable spikes or water pressure step changes that were considered, upon examination, to be the result of a temporary measurement error.

The review of the piezometers and INAs resulted in 57 data points (i.e., 41 piezometers and 16 INAs) being considered for calibration. Figure 23 shows the location of the selected piezometers, INAs, and CPTu used in the calibration.

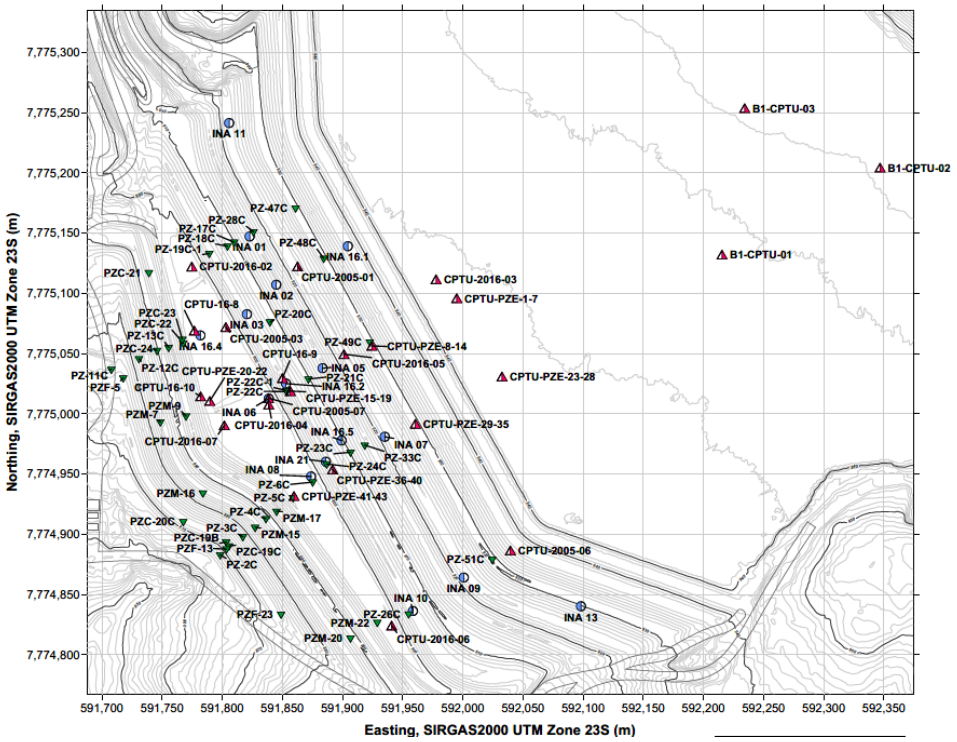

Figure 23: Location of Selected Piezometers, INAs, and CPTus Used for Seepage Calibration

4.6.1.1 Water Level Trends

The piezometer and INA data were reviewed to determine: (i) any annual trends in the data; and (ii) the trend in 2018 and leading up until the failure.

To determine whether there was a noticeable annual trend in all piezometer readings, the readings were zeroed out at the start of each calendar year. Then, the difference in each reading was plotted. This did not show a discernable annual trend. In addition, there did not appear to be a clear correlation to rainfall data. This was expected due to the buffering influence of the unsaturated zone and the depth at which the piezometers were installed.

To evaluate changes in water levels in the dam, the piezometer and INA readings were grouped by location. The grouping comprised all instruments located on the dam either above or below elevation 900 meters above mean sea level (m msl). This essentially combines piezometers and INAs that were either installed above the setback or on and below the setback. The resulting mean water levels measured during the three years prior to failure are plotted on Figures 24 and 25. Figure 26 shows results from all the piezometers and INAs. The data were referenced to the final reading in January 2019.

The results show that there was a gradual decline in the mean water level since 2016. The decline was about 1.4 m for the installations above the setback (900 m msl) and about 0.5 m for the installations on or below the setback. This observation is attributed to a slow net drawdown of water after tailings deposition ceased in 2016. The water appears to be draining from the upper portions of the dam toward the lower portions. The drawdown also creates an increasing unsaturated zone in the upper portions of the dam. The results also show minor short-term increases in water level that appear to be linked to responses during the wet seasons.

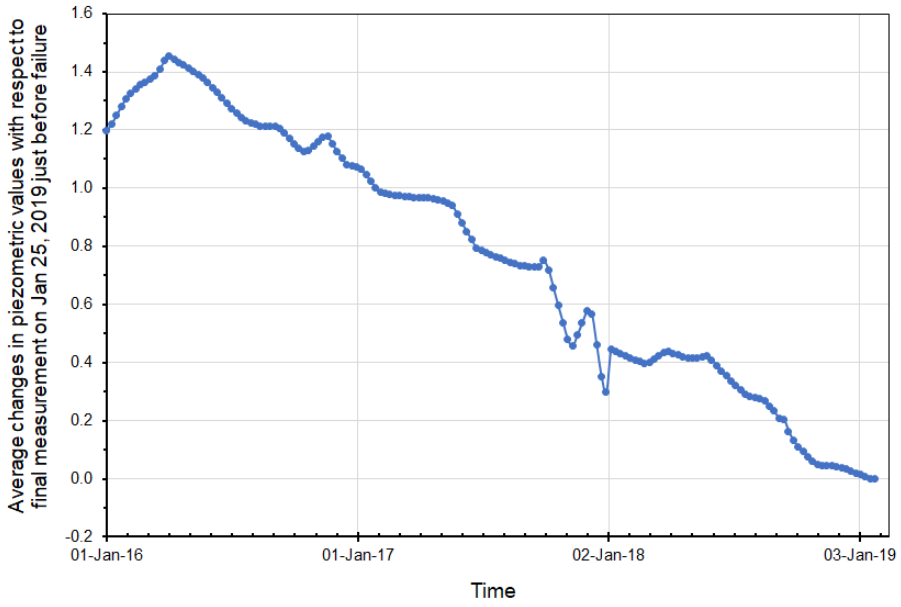

Figure 24: Changes in Piezometer and INA Readings Above Elevation 900 m msl

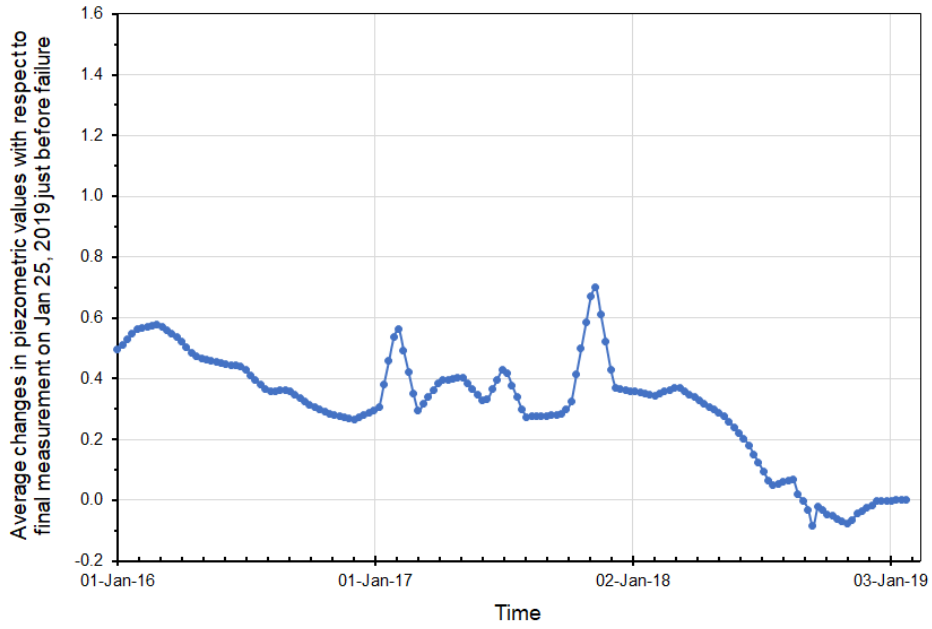

Figure 25: Changes in Piezometer and INA Average Readings Below Elevation 900 m msl

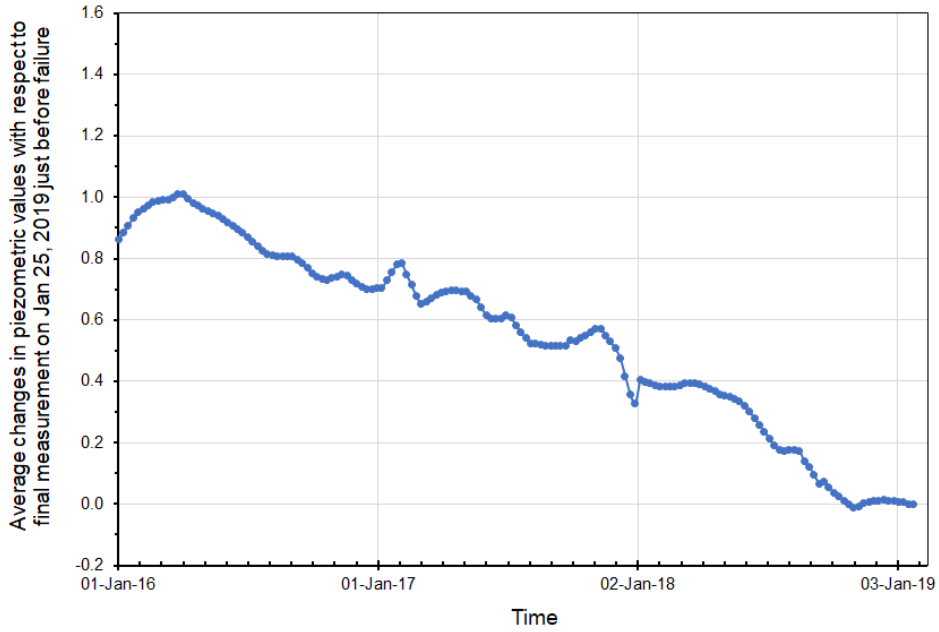

Figure 26: Average Changes in Piezometer and INA Readings for All Piezometers and INAs

4.6.2 CPTu data

The CPTu data were used along with the piezometer and INA readings for calibration. Dissipation testing was performed at various depths for the CPTu data collected at the site and was therefore integrated into the calibration study. CPTu data collected during 2016 and 2018 were utilized even though there may be a difference associated with the gap between the collection time and January 2019. Given the small (< 1.2 m) three-year decline in water levels in the piezometers, it was considered that CPTu data collected during the 2016 and 2018 calendar years represented a good source of data which could be utilized to calibrate the January 2019 seepage model.

CPTu data primarily existed along the central region of the dam, as shown in Figure 23. CPTu data that did not exactly fall on cross-sections were projected onto the nearest cross-section.

An overall downward gradient of approximately 50% of hydrostatic was observed as a global average for the CPTu data.

4.7 Pre-failure January 2019 Steady-state Calibration

Calibration was performed to align the numerical modeling with the observed field conditions and laboratory measured properties. The approach was to calibrate a steady-state model to the pore pressure readings close to January 2019. The calibration included 2D cross-sections 1-1, 2-2, and 3-3. A detailed geometry was utilized for the calibration that included a separation of the tailings into coarse, fine, and slimes zones.

The manual back-analysis primarily involved the modification of the following elements to match field measurements:

- Infiltration rate of 50% of 1400 mm annual rainfall;
- Drain locations;
- Anisotropic permeabilities;
- Foundation permeability; and
- Reasonable pond location.

The results of this process are described in the following sections.

4.7.1 2D Calibration

Manual calibration to cross-sections 1-1, 2-2, and 3-3 are presented in the following sections. The calibration to all cross-sections was performed as a steady-state calibration to piezometers and INA data in January 2019 and CPTu data from 2016 to 2018. The final piezometer readings prior to failure were utilized in the calibration. Calibration was performed to piezometer/INA/CPTu data simultaneously. A top boundary condition of 50% of 1400 mm/year rainfall was applied to the top boundary of the model to represent the net effect of rainfall and evaporation.

4.7.1.1 Cross-section 1-1

The final cross-section geometry for cross-section 1-1 can be seen in Figure 27. The figure also projects the location of piezometers, INAs, and CPTu instruments that were utilized for the calibration onto the profile.

The results of the calibration for cross-section 1-1 can be seen in Figure 28. The pond boundary condition was set 300 m back from the crest of the top berm as an approximation of the 3D pond location. Numerical models with k_h/k_v = 5 and 10 were analyzed, and the best calibration was obtained with a k_h/k_v = 5. A foundation permeability of 9.3×10^{-7} m/s provided the best calibration. The INA heads measured are overlain on the model with a light blue line. The pressures measured in the piezometers and CPTu instruments are represented with a horizontal line that is colored the same color scheme as the pore water pressure contour color scheme. This display allows visual identification of the consistency between field and model results all displayed in terms of pressure units in kPa.

The location of the CPTu instruments utilized in the calibration for cross-section 1-1 can be seen in Figure 29. The comparison of model results plotted against CPTu provided reasonable collaboration with the measured data as shown in Figure 30.

The overall correlation between field and model results for INAs, piezometers, and CPTu data may be seen in Figure 31 that produces a correlation coefficient (R^2) value of 0.95.

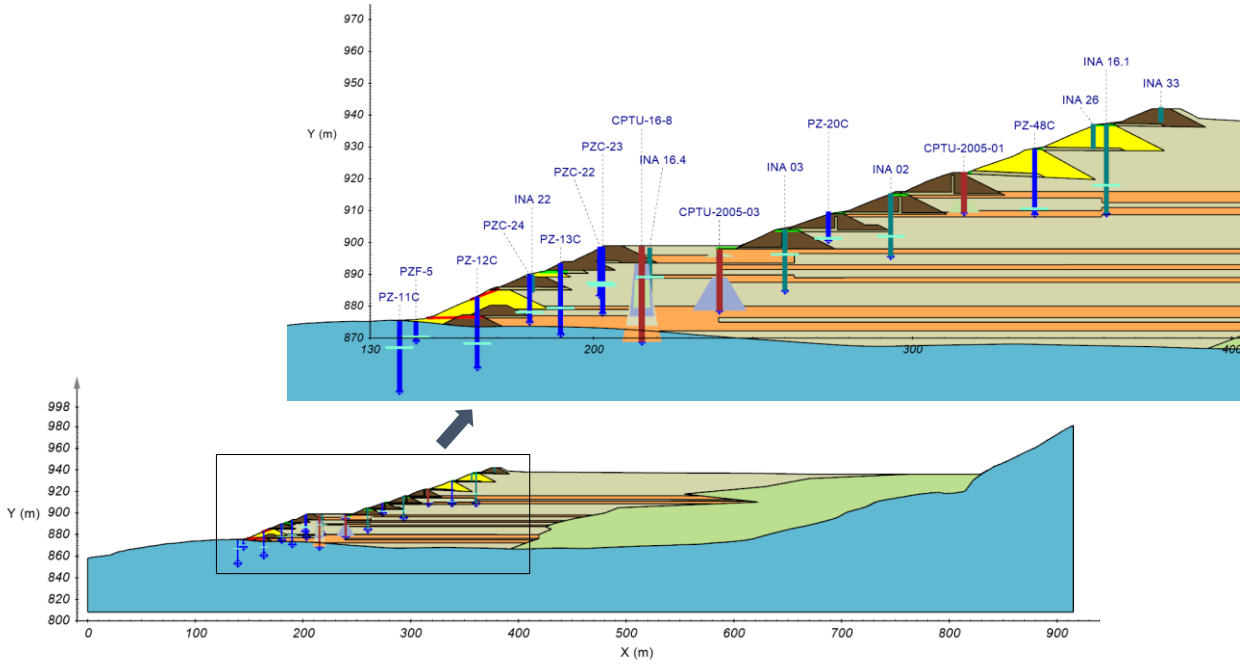

Figure 27: Geometry of Cross-section 1-1 Including Piezometers, INA, and CPTu Data

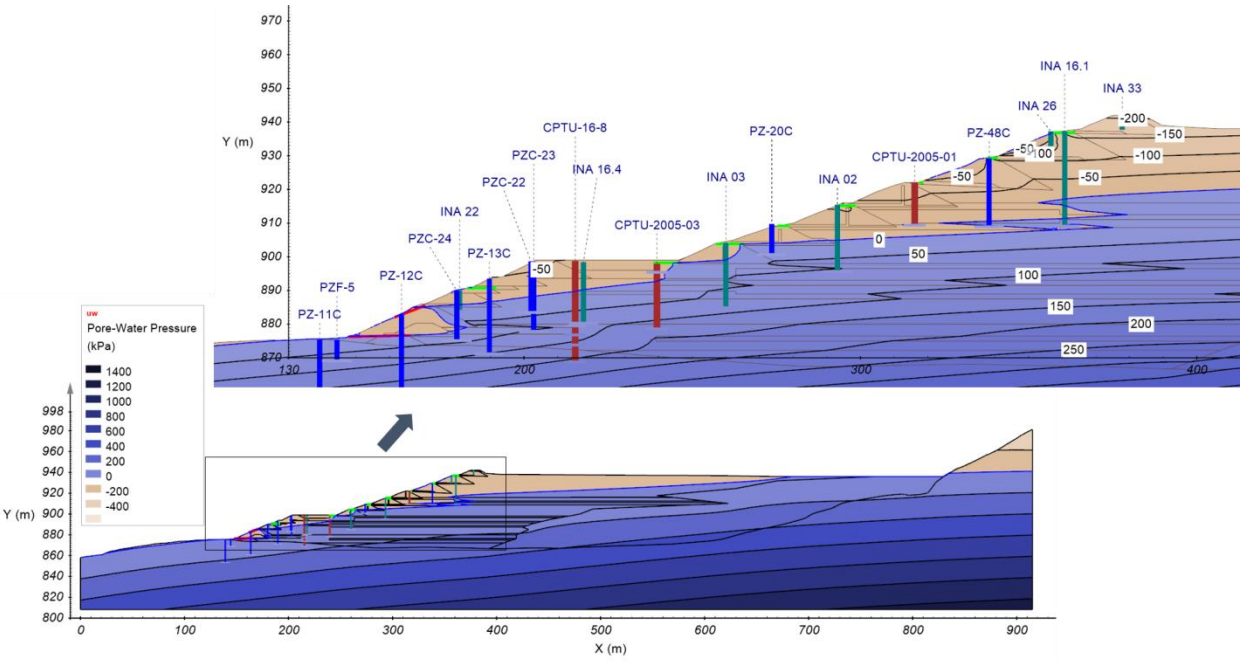

Figure 28: Calibration to Groundwater Flow for Cross-section 1-1

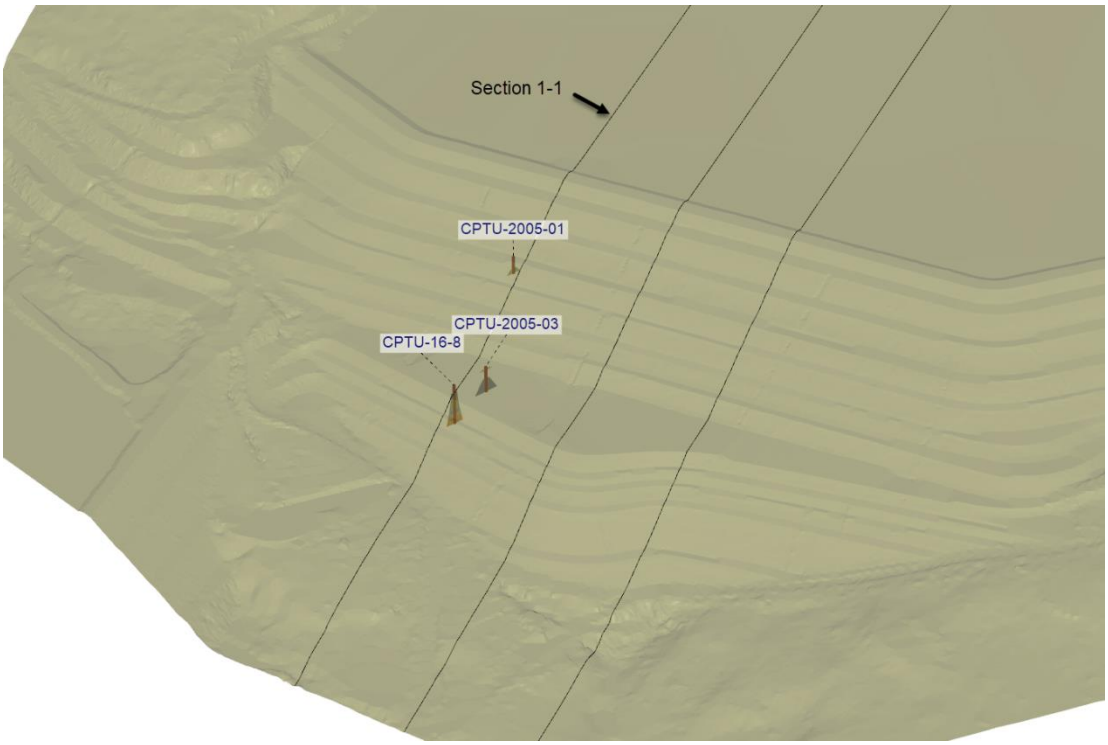

Figure 29: CPTu Locations Used to Calibrate Cross-section 1-1

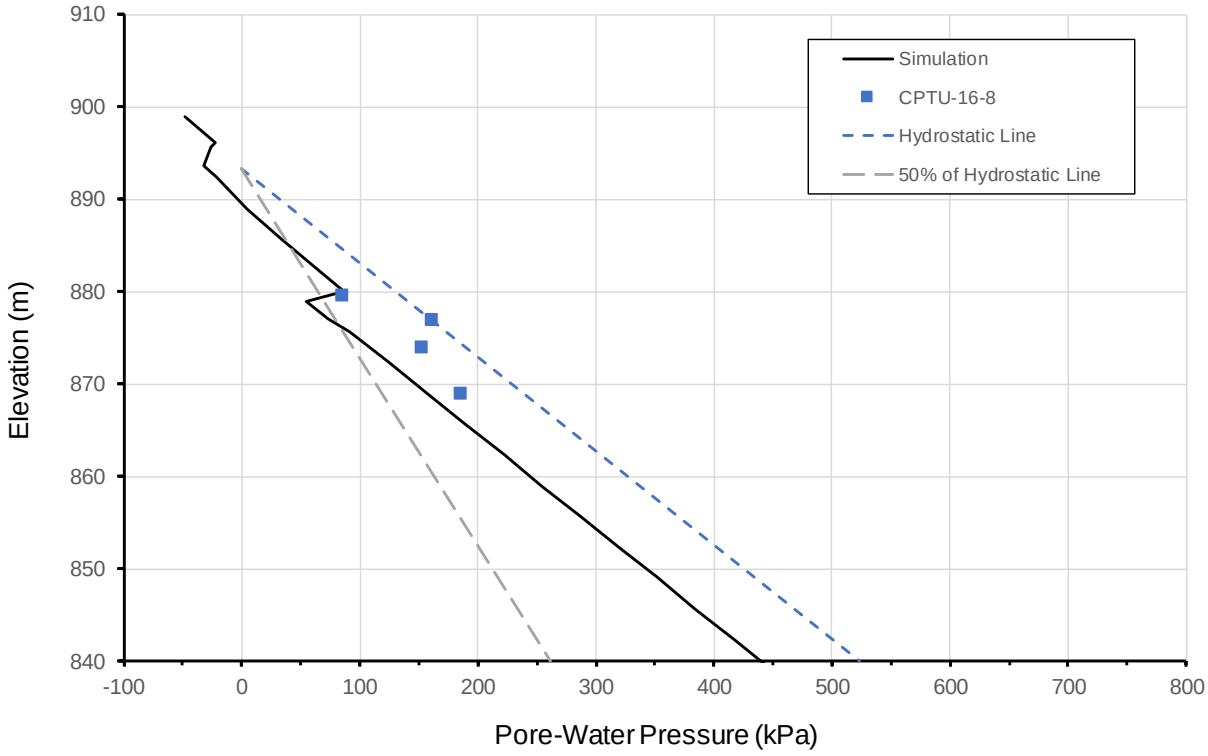

Figure 30: Example Calibration to CPTu Data on Cross-section 1-1

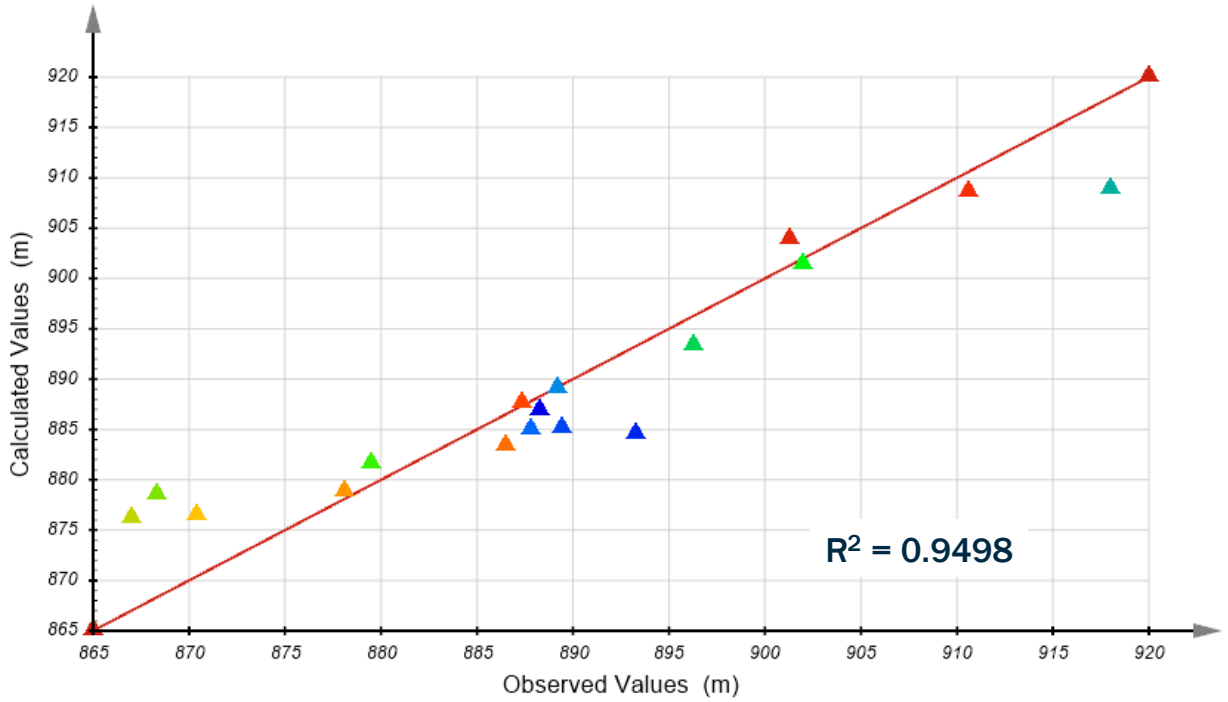

Figure 31: Difference Between Observed and Model-calculated Heads for Cross-section 1-1

4.7.1.2 Cross-section 2-2

The geometry and location of the nearby piezometers, INAs, and CPTu locations for cross-section 2-2 may be seen in Figure 32. The cross-section had more instrumentation installed than cross-section 1-1 and therefore allowed instrumentation comparison in more detail. CPTu pore pressure dissipation testing is plotted as triangles with the bottom of the triangle indicating the location of the reading and the top of the triangle representing a projected zero pore water pressure condition.

The resulting pore pressure distribution can be seen in Figure 33. The results show the potential lateral seepage around Elevation 930 m msl due to the fine tailings layer. The water table is shown to be close to the ground surface at around 900 m msl. The location of the fine tailings layers in the model shows the possibility for the development of perched saturation zones in the model (Elevation ~930 m msl). The pressure readings in the piezometers also show reasonable agreement with the contours of model pressures. Higher water pressures are noted in the Starter Dam where there is no drainage. The water table shows as daylighting on the downstream slope of the Starter Dam.

The CPTu measurement points are shown in Figure 34. In this cross-section there are 12 CPTu measurement points that are close to the cross-section and were utilized for the calibration. An

example calibration can be seen in Figure 35. Some discrepancy with the data was noted that was primarily due to variations between the field and model water table. Overall the alignment of CPTu data with the model results was better when $k_h/k_v = 5$ for the coefficient of permeability was utilized.

The correlation coefficient (R^2) value between model results and all CPTu, piezometers, and INA data was 0.965 and can be seen in Figure 36.

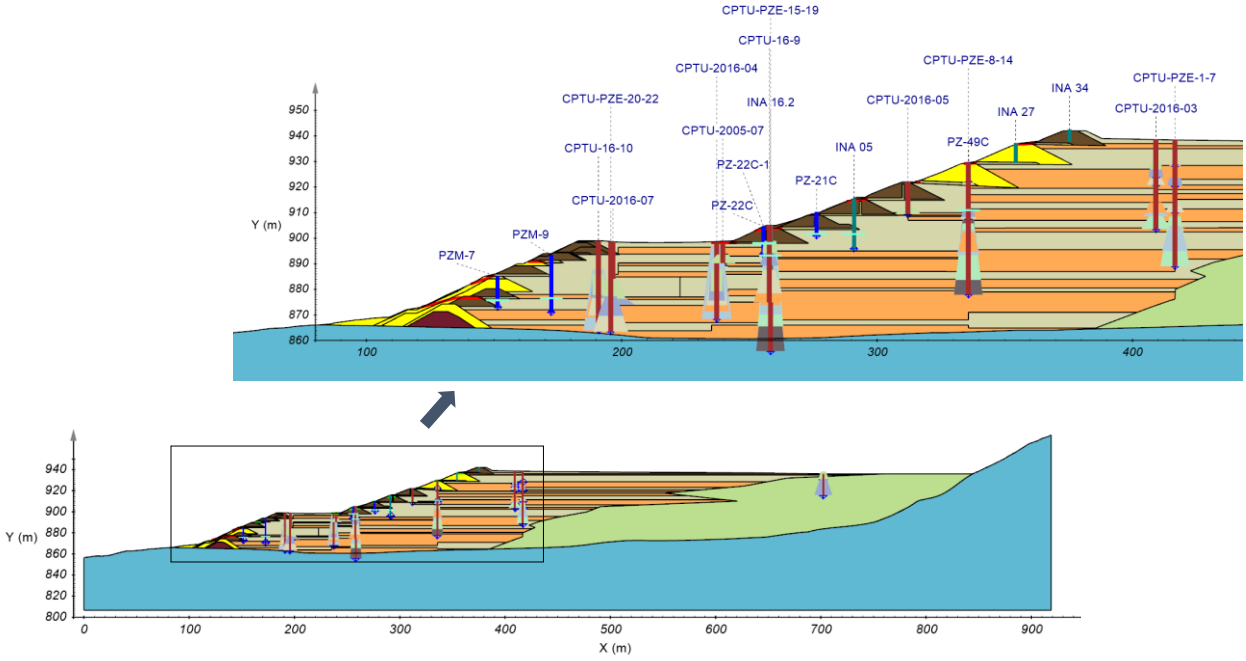

Figure 32: Geometry of Cross-section 2-2 Including Piezometer, INA, and CPTu Data

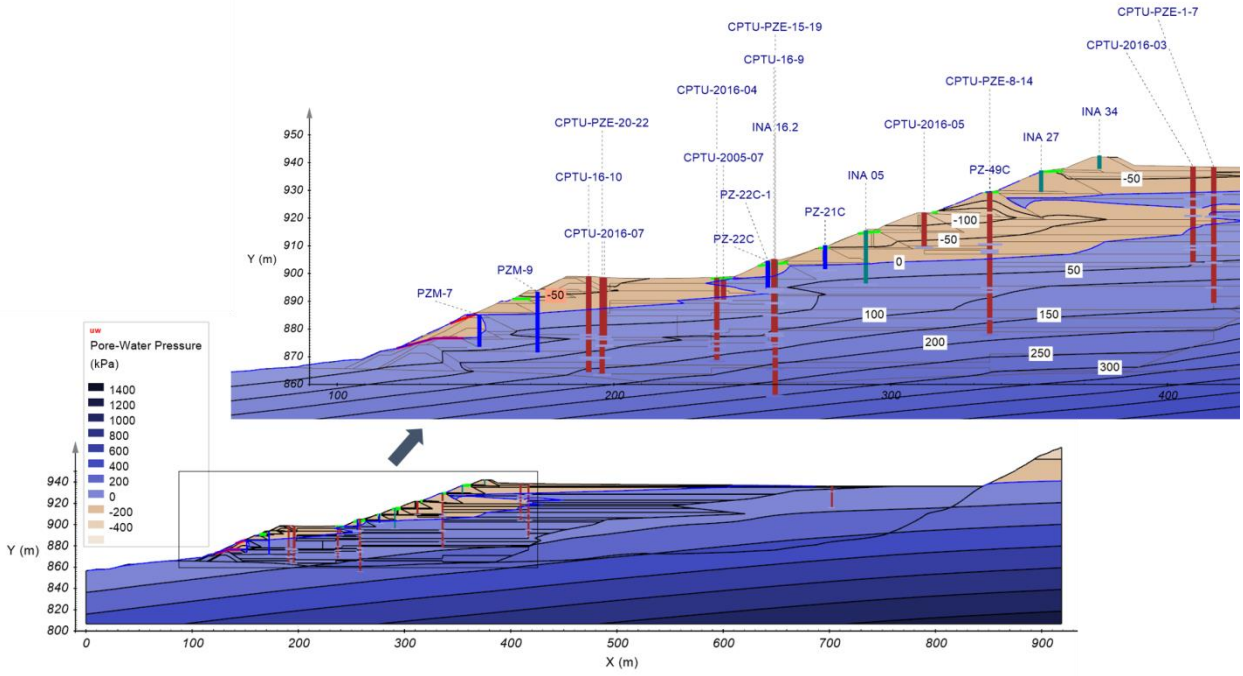

Figure 33: Calibration to Groundwater Flow for Cross-section 2-2

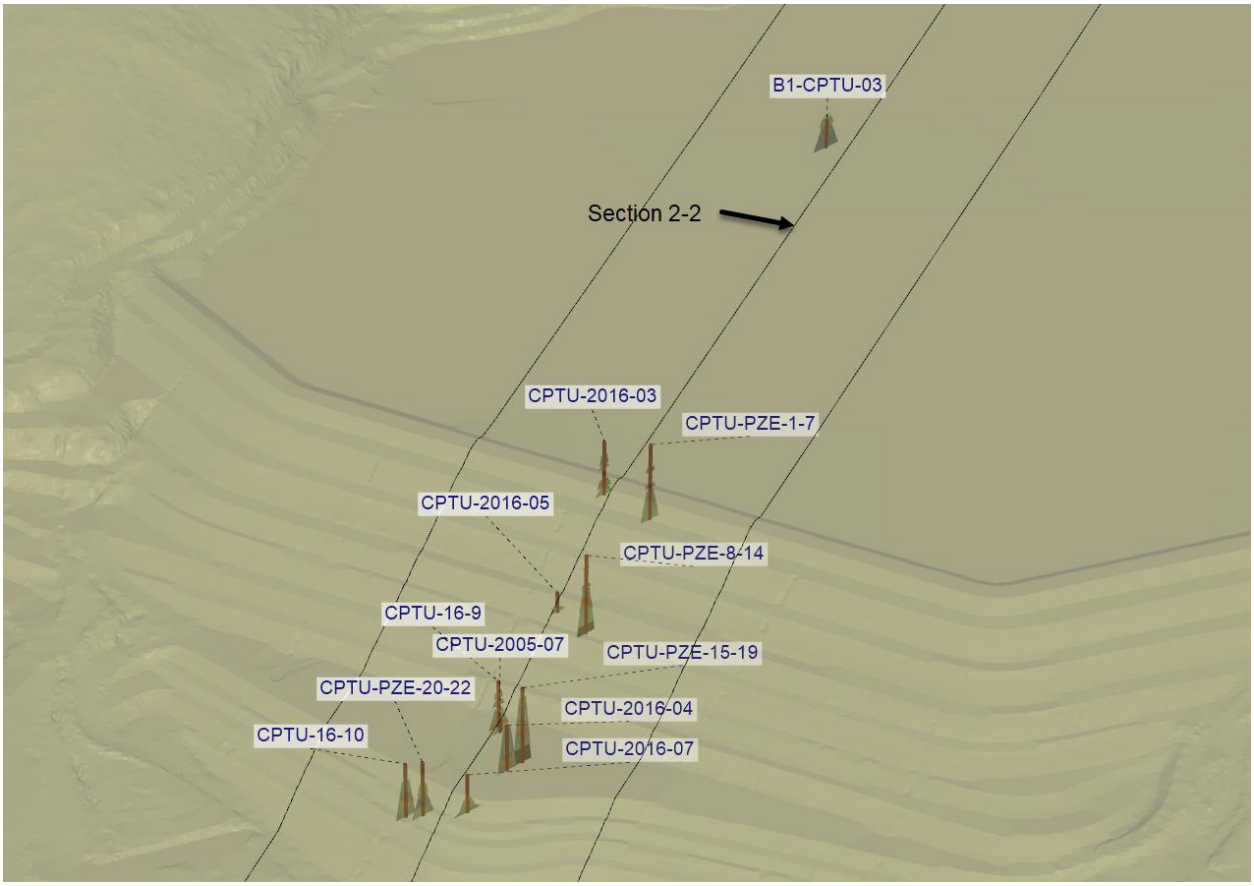

Figure 34: CPTu Locations Utilized for Calibration of 2D Model Along Cross-section 2-2

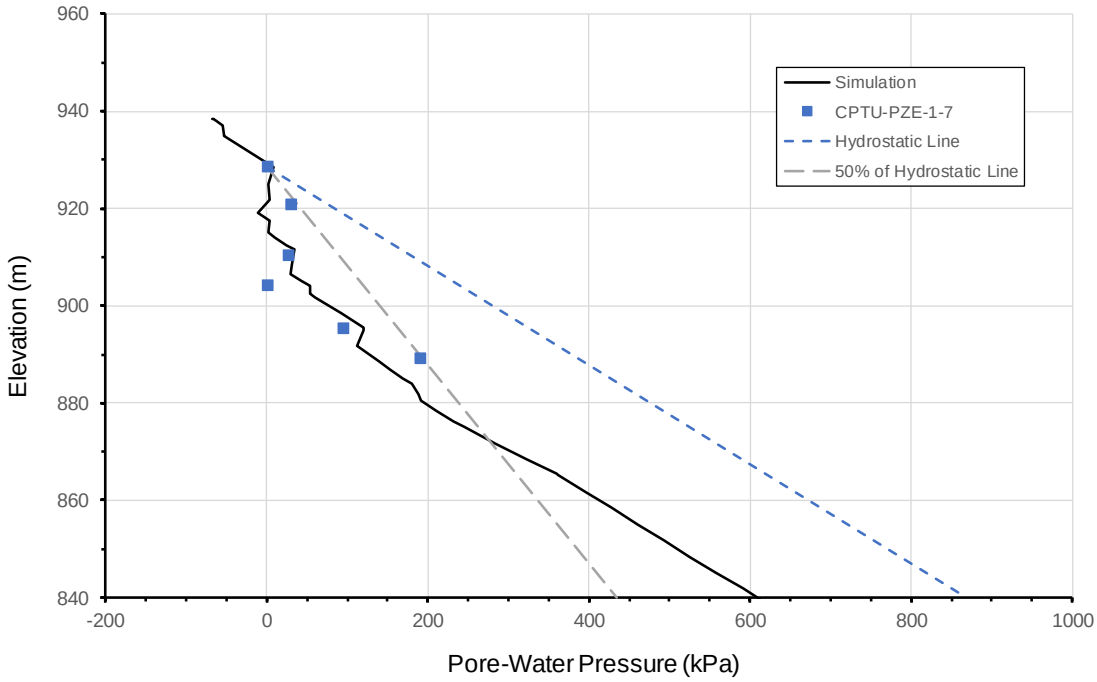

Figure 35: Example CPTu Profile and Comparison to Seepage Pore Water Pressure Results

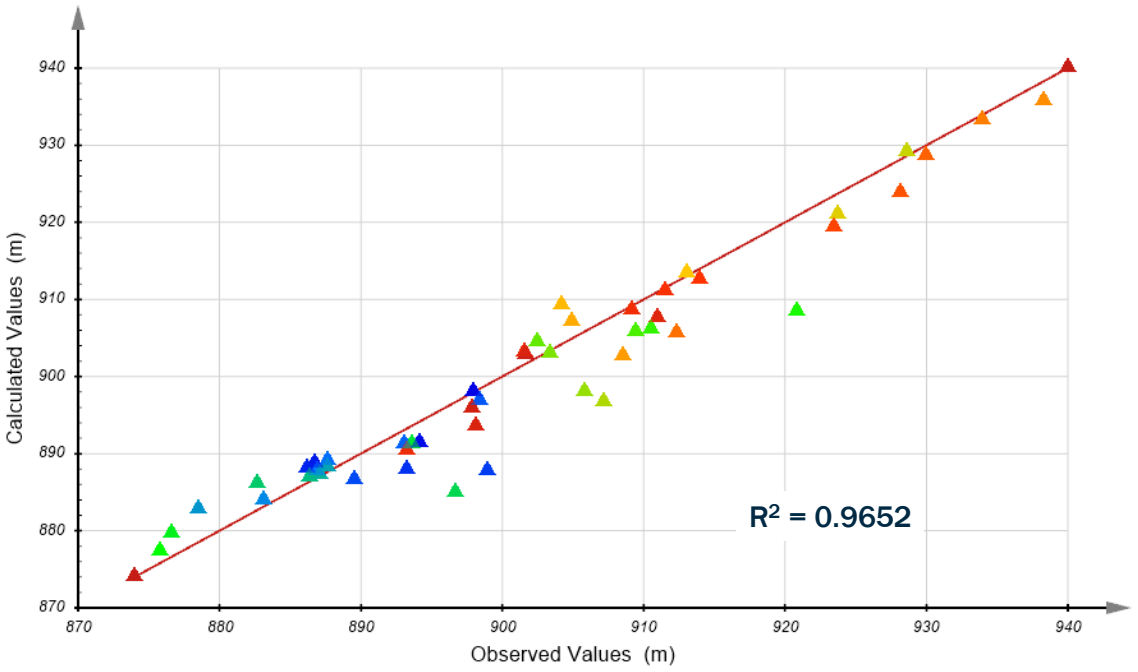

Figure 36: Difference Between Observed and Model-calculated Heads for Cross-section 2-2

4.7.1.3 Cross-section 3-3

Cross-section 3-3 contains a number of piezometers and CPTu profiles that provided an opportunity to calibrate to the measured values. The profile including fines/coarse/slimes may be seen in Figure 37 as well as the piezometer, INA, and CPTu locations. Instruments close to the profile were projected onto the profile for calibration purposes.

The calibrated model is shown in Figure 38. The water table is high at Elevation 900 m msl, and the drains assumed to have been installed in the Second Raising allow for a reasonable calibration to field data below 900 m msl. A water table higher than the one calculated would provide a slightly better fit to the data behind the dam crest berm, but the layering of coarse and fine materials and the related coefficient of permeabilities dictate the location of the water table.

Six CPTu profiles were used to calibrate the model, and their locations are shown in Figure 39. The CPTu data calibrated well with measured values (see example in Figure 40) and confirmed the initial estimate of the pore water pressures being at about 50% of hydrostatic values. The effect of the fine/coarse layering can be seen in the pore water pressure profile results.

The overall R^2 calibration result is shown in Figure 41 and can be considered excellent. The related final coefficient of permeabilities and anisotropy values based on the calibrations are shown in Table 4.

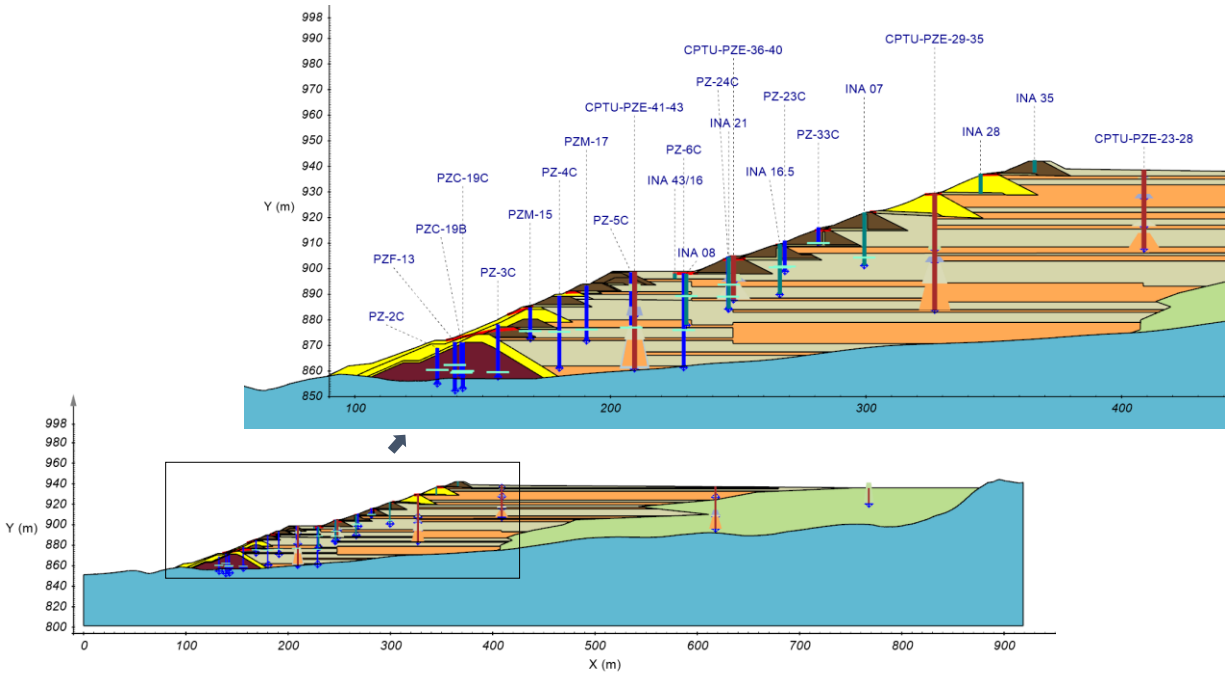

Figure 37: Geometry of Cross-section 3-3 Including Piezometer, INA, and CPTu Data

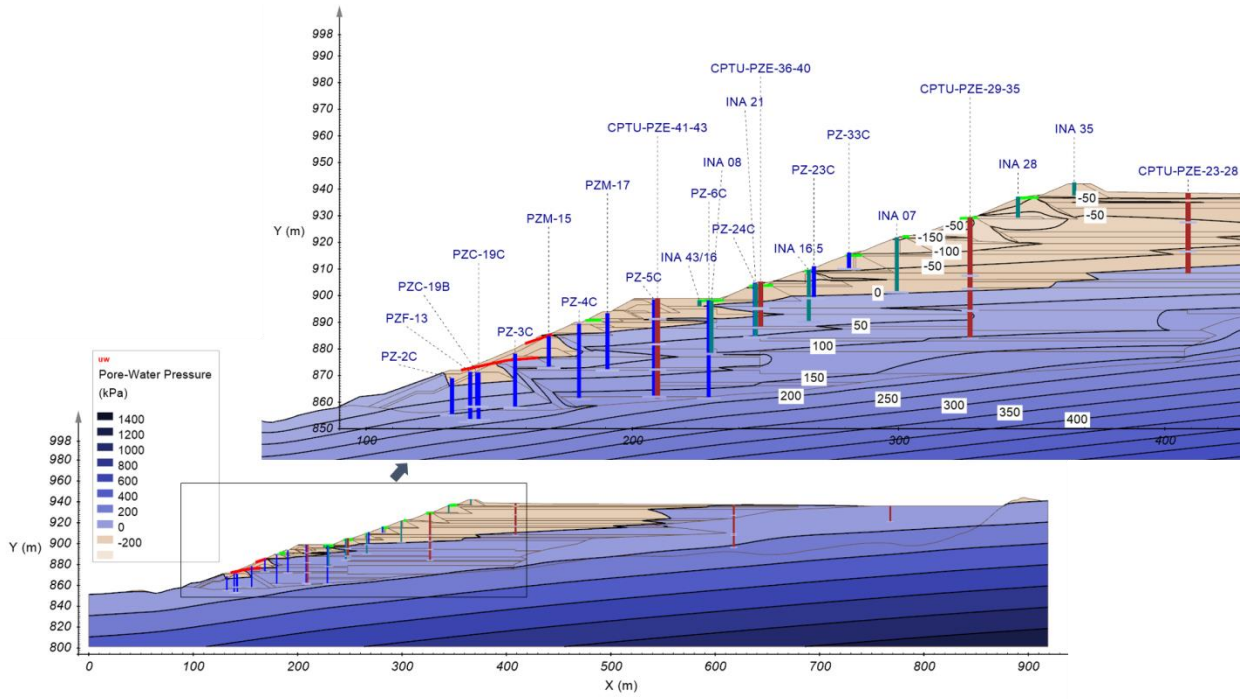

Figure 38: Calibration to Groundwater Flow for Cross-section 3-3

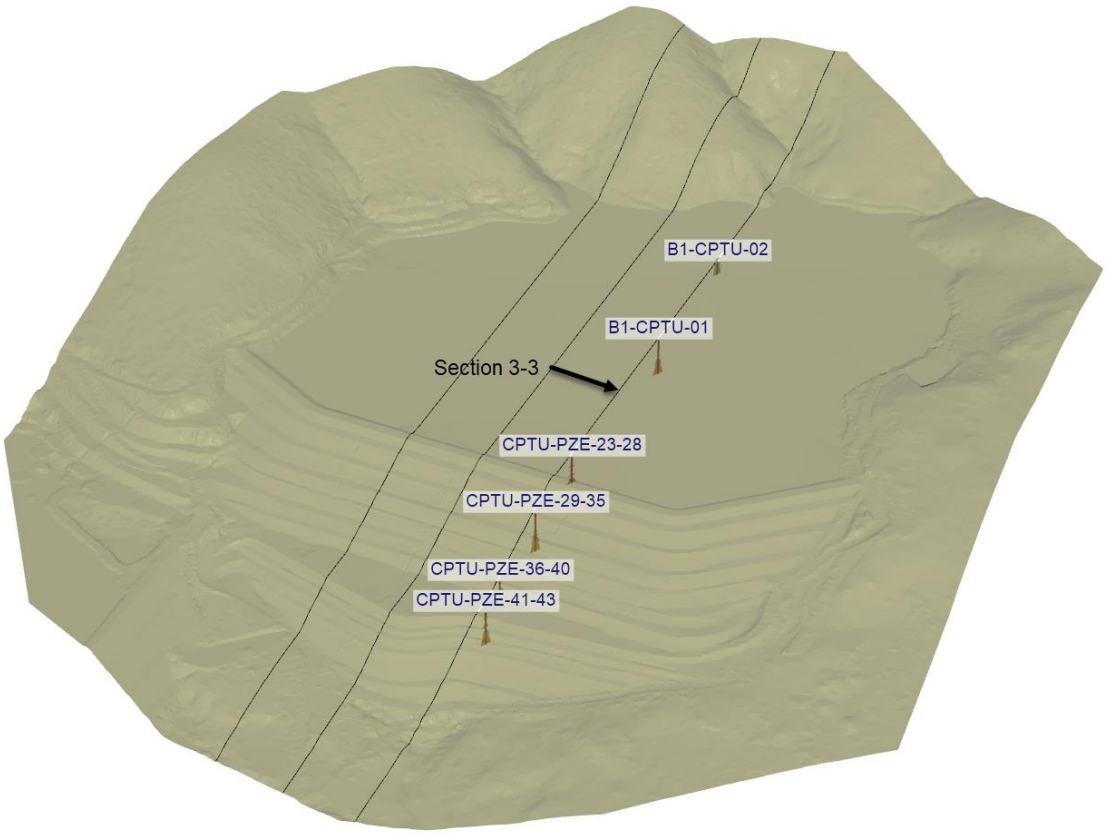

Figure 39: CPTu Instruments Used to Calibrate Cross-section 3-3

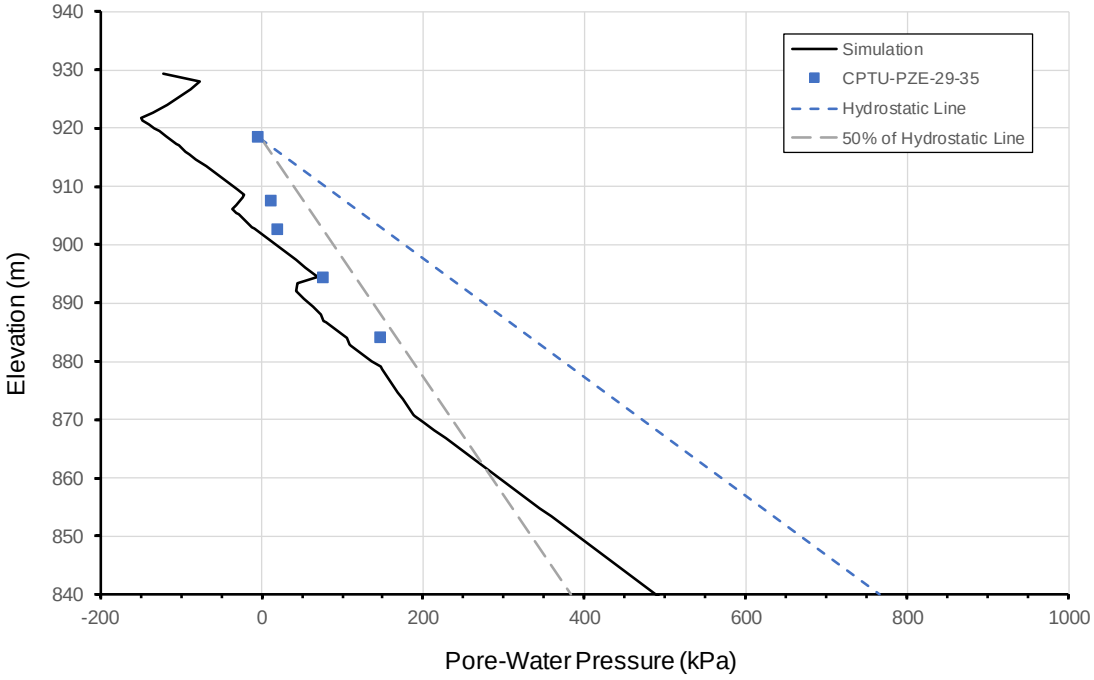

Figure 40: Example Calibration to CPTu Data on Cross-section 3-3

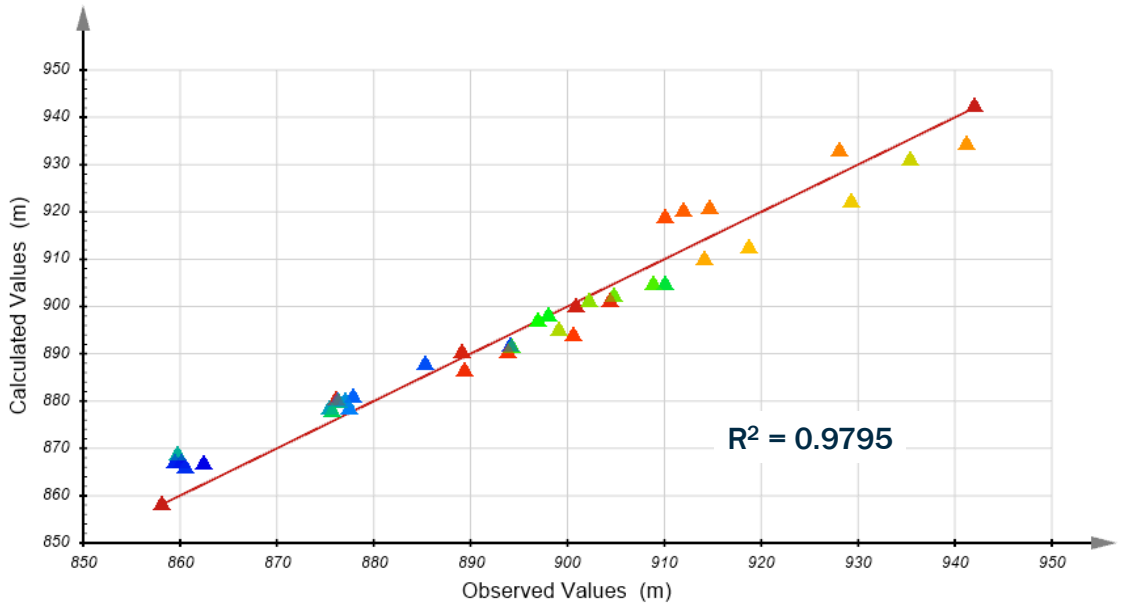

Figure 41: Difference Between Observed and Model-calculated Heads for Cross-section 3-3

Table 4: Final Calibrated Saturated Permeabilities for All 2D Cross-sections

Material	**Horizontal Permeability (k_h, m/s)**	**Vertical Permeability (k_v, m/s)**	**Anisotropy (k_v/k_h)**
Foundation soil	9.3×10^{-7}	9.3×10^{-7}	1
Drainage	1×10^{-4}	1×10^{-4}	1
Compacted tailings	5×10^{-7}	1×10^{-7}	0.2
Compacted soil	1.2×10^{-9}	1.2×10^{-9}	1
Ultrafine iron ore	1.2×10^{-6}	1.2×10^{-6}	1
Fine tailings	1×10^{-7}	2×10^{-8}	0.2
Coarse tailings	5×10^{-6}	1×10^{-6}	0.2
Slimes	1×10^{-8}	2×10^{-9}	0.2

4.7.1.4 Water Balance – 2D

A water balance calculation was performed for all calibrated models. The water balance clarified the quantities of flow coming in by rainfall and entering the model through the pond. Water could then exit the model through the downstream foundation or through the installed drains in the dam structure.

The amount of infiltration that enters the model on the tailings beach is dependent on the material near the surface. In cross-section 1-1, the top surface is comprised entirely of coarse tailings and therefore 100% of applied flow enters the model, as shown in Figure 42. In cross-section 2-2, the runoff is 8.2% and in cross-section 3-3, the runoff is 22%.

The majority of flow leaving the system is through the drains installed in the dam structure or through the downstream foundation as shown in the water balance in Figure 43. The amount of

water entering through the slimes via the pond is significantly lower than the infiltration on the beach area due to rainfall. Runoff is higher on the berms due to the lower permeability of dam materials.

Drain flows from all the drains are 4.53×10^{-2} m^3/hr, 3.49×10^{-2} m^3/hr, and 3.13×10^{-2} m^3/hr, in the models of cross-sections 1-1, 2-2, and 3-3, respectively. Overall, the model solved with a net water balance error close to 0%.

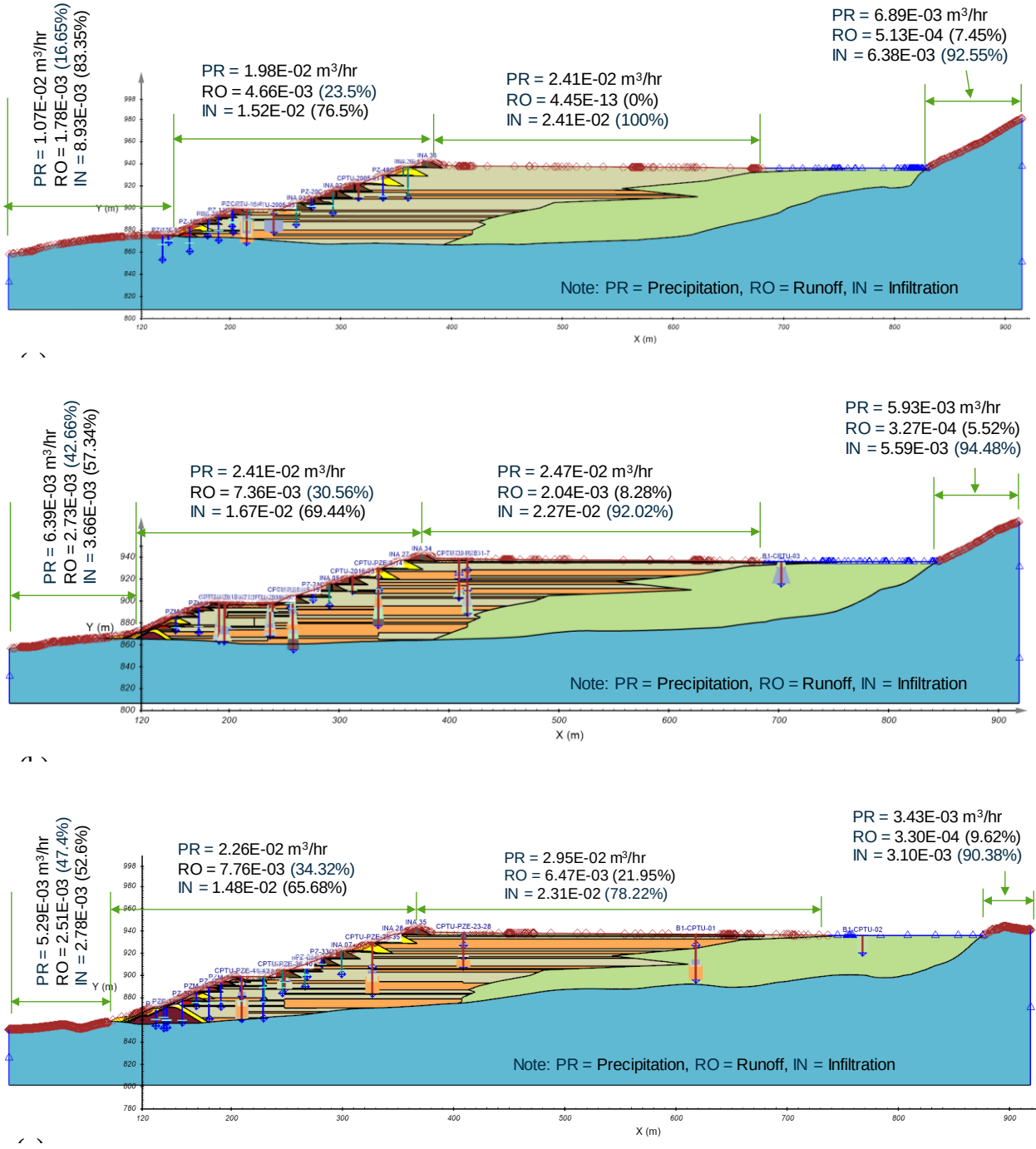

Figure 42: Summary of Climate Water Balance (With 50% Rainfall): (a) Cross-section 1-1; (b) Cross-section 2-2; and (c) Cross-section 3-3

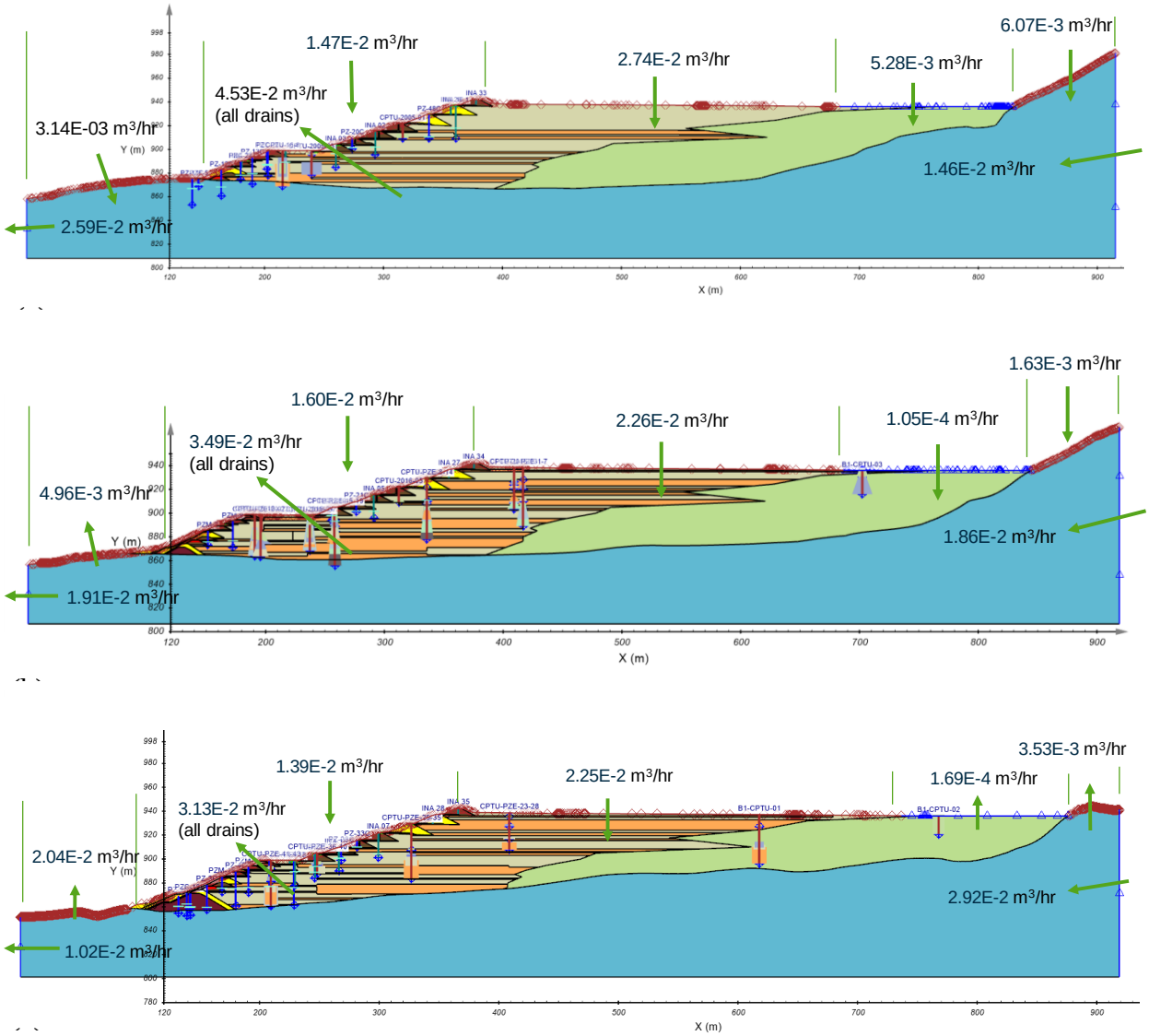

Figure 43: Summary of Water Balance: (a) Cross-section 1-1; (b) Cross-section 2-2; and (c) Cross-section 3-3

4.7.2 3D Calibration

A 3D model was also created to evaluate the flow regime that allows a better representation of the curved structure of the dam, the underlying natural ground topography, and the location of drains in the model. Material properties, infiltration rate, and layering utilized for the 3D seepage model were the same as those utilized in the 2D computer model.

The 3D model represented the detailed 3D aspects of the site, including the DHPs and the blanket/chimney drains. A 3D model was created reflecting the heterogenous nature of the tailings. The bulk anisotropy of $k_h/k_v = 5$ from the 2D model calibration was used for the three tailings materials in the 3D model. The material properties utilized in the model can be seen in Table 4.

The model was set up with the following conditions:

- 50% rainfall with the run-off correction method applied;
- Saturated material properties;
- 12 DHPs included (i.e., internal boundary conditions applied).

Calibration was completed to the following data:

- 41 piezometers (September 2018 – January 2019);
- 16 INAs (September 2018 – January 2019); and
- 84 CPTu dissipation test readings (2016 and 2018).

The results of the model are demonstrated in Figure 44 and Figure 45. A large beach length was formed on the tailings surface, and the water table daylights only on the Second and Third Raises. The water table is slightly lower (Figure 38) than the 2D counterpart. This was to be expected, given the difference in the location of the pond between the 2D and 3D models. The calibration of the existing model was good as shown in Figure 45.

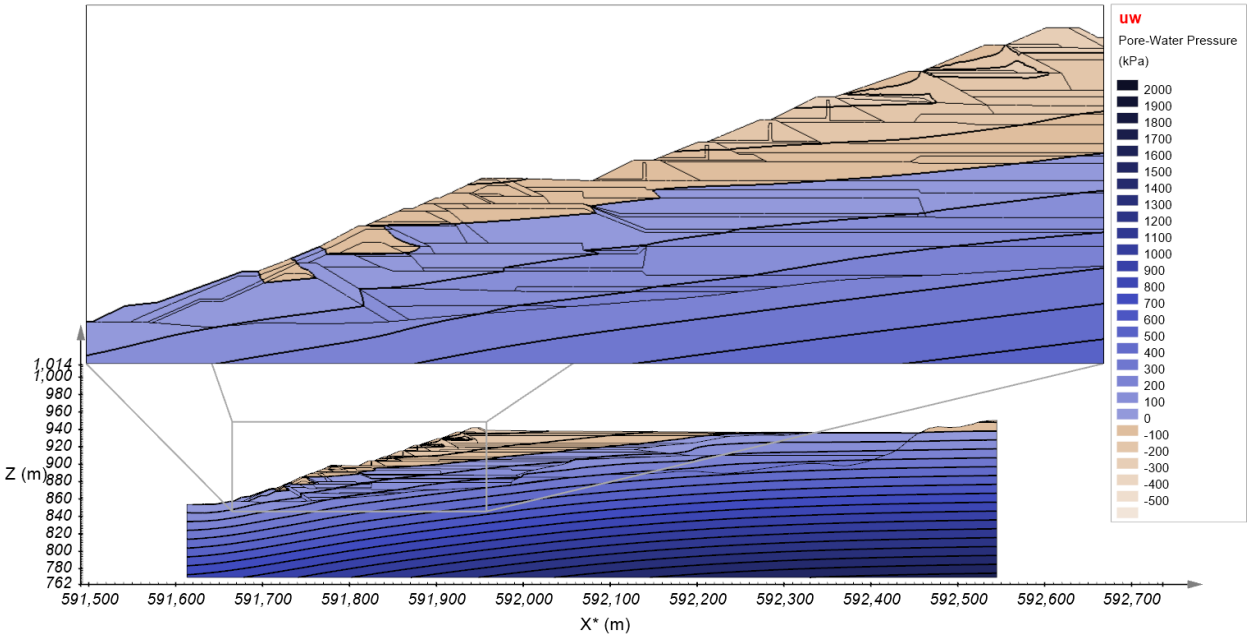

Figure 44: Display of Water Table in 3D Model Along Cross-section 3-3

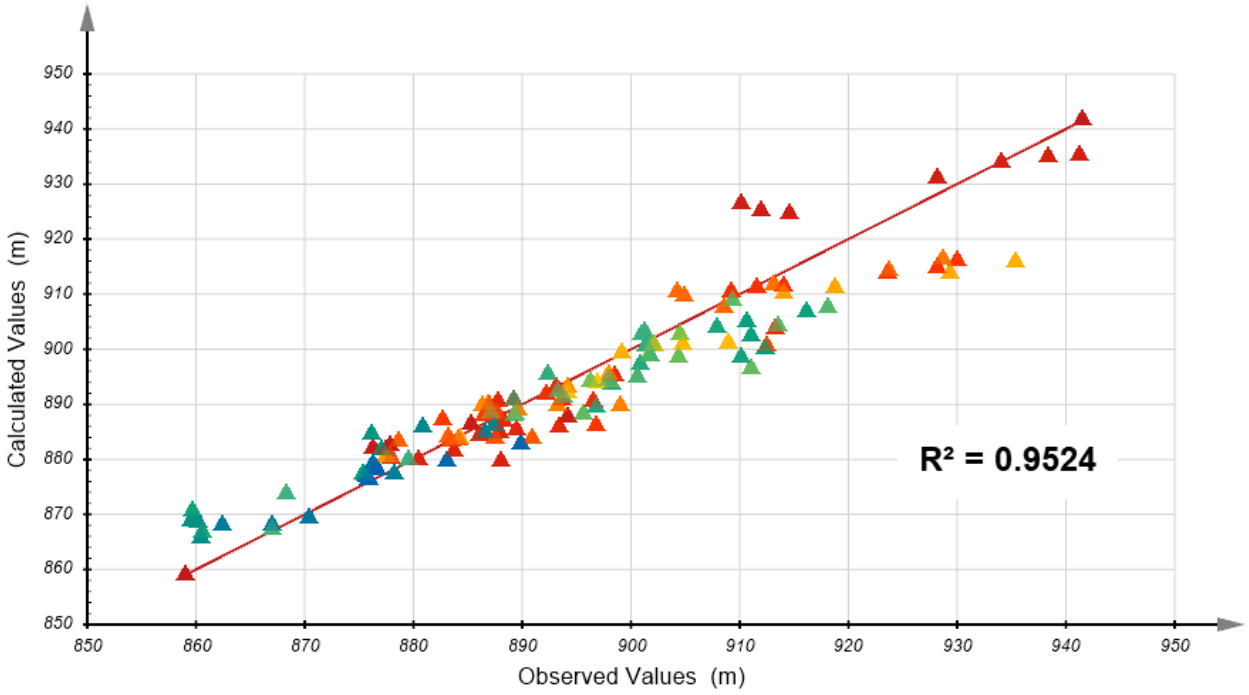

Figure 45: R^2 value Calculated for 3D Heterogeneous Model

4.7.2.1 Water Balance – 3D

The water balance was also computed for the 3D model. The water balance for the climatic boundary condition with 50% of annual average rainfall applied on the top surface of the model is presented in Table 5. The numbers presented in Table 5 include the climatic effect on the entire top surface of the 3D model, which includes the tailings surfaces, berms, and surrounding 10% to 15% foundation area included in the 3D model. The 3D model contains coarse tailings as the top surface material for the majority of the tailings area.

Table 5 shows that most water flowed through the downstream foundation in comparison to the flow from drains and DHPs. The total drainage flow including from the drains and DHPs is about 8 m^3/hr from the 3D tailings model (Table 5), which is comparable to the average total flow of about 10 m^3/hr in 2018 (see Appendix C for individual flow rates at each drain). Similar to the 2D model (Section 4.7.1.4), the inflow from the pond is negligible in the 3D models. This was expected because the pond is on top of slimes that have a low permeability (Table 3).

Table 5: Summary of Comprehensive Water Balance for 3D Calibration Model

Surface Boundary	Inflow (m^3/hr)	Outflow (m^3/hr)
Upstream foundation	38.81	
Pond	1.90E-03	
Entire top surface (including tailings, berms, and surrounding area)	21.29	
Deep horizontal pipes		3.04
Drains		4.95
Downstream foundation		52.11
Total	60.10	60.10

4.7.3 Calibration Summary

In summary, the manual calibration process yielded a reasonable calibration to all known field measurements of pore water pressure from INAs, piezometers, and CPTu tests and offered a reasonable calibration to drain flow. Calibration to three 2D cross-sections as well as a full 3D model provided assurance that the seepage model is matching field results in a reasonable manner.

5 SEEPAGE MODELING FOR PREDICTING CONSTRUCTION STAGES

This section presents the results of predictive scenarios for transient unsaturated 2D analysis and various 3D construction stages utilizing material properties and boundary conditions from the calibrated models.

5.1 Transient Unsaturated 2D Analysis for 2016-2019

Transient 2D model runs were performed to determine pore water pressure distribution in the three years leading up to the failure. The modeling was set up as follows:

- Unsaturated flow based on SWCCs;
- Soil anisotropy of tailings k_v/k_h = 0.2 (based on steady-state calibration results presented in Section 4.7.1);
- Hourly rainfall data was applied with 50% infiltration;
- Cross-sections 1-1, 2-2, and 3-3 were modeled;
- Modeling time was from January 2016 to January 2019;
- Initial conditions were established from a steady-state saturated model using 50% average annual rainfall (1400 mm/year);
- Actual hourly rainfall data from combined F11 (2016) and F18 (2017-2019) automated rain gauges were applied to the top of the entire model;
- Head = 941 m on upstream foundation;
- Head = 856.21 m on downstream foundation; and
- Head = 936 m for pond on tailings.

Pore pressure conditions demonstrate a divide between the saturated and unsaturated zones. The water table was found to slowly decrease by approximately 2 m to 4 m over the three years, which is consistent with an average decrease of 1.6 m in piezometric values recorded by field piezometers and INAs situated above 900 m msl. However, the suctions above the water table decreased due to the rainfall encountered in 2016. The 2017 average rainfall and the 2018 higher than average rainfall furthered the advance of water flow into the system that decreased suctions in a top-down manner shown in Figure 46. Suctions decreased from an average of between 35 kPa and 75 kPa to between 5 kPa and 20 kPa over the three-year period. The vertical downward movement of water is governed by the combined effects of the fine and coarse material vertical permeability. The bottom of the reduced suctions zone reaches approximately 25 m depth after the three years modeled. Figure 47 shows the computed reduction in shear strength associated with the advance of the wetting front. The decrease in shear strength in the unsaturated zone was calculated using

the method described by Fredlund, Xing, Fredlund, and Barbour (1996)[12] over three years leading up to the failure on January 25, 2019.

In summary, the analysis shows:

The model agrees with the observed decrease in water levels in the three-year period from 2016 to 2019.

- The 50% of hydrostatic pore pressure profile with depth is a reasonable approximation (particularly at the critical elevation of the setback).
- There is a difference in behavior between the unsaturated zone and the saturated zone.
- The unsaturated zone was progressively wetting-up.
- A net average reduction in the shear strength of the unsaturated zone of up to 15 kPa was realized progressing down to a depth of 25 m after three years.

[12] Fredlund, D.G., Xing, A., Fredlund, M.D., & Barbour, S.L. (1996). The relationship of the unsaturated soil shear strength function to the soil-water characteristic curve. *Canadian Geotechnical Journal*, *33*(3), 440-448.

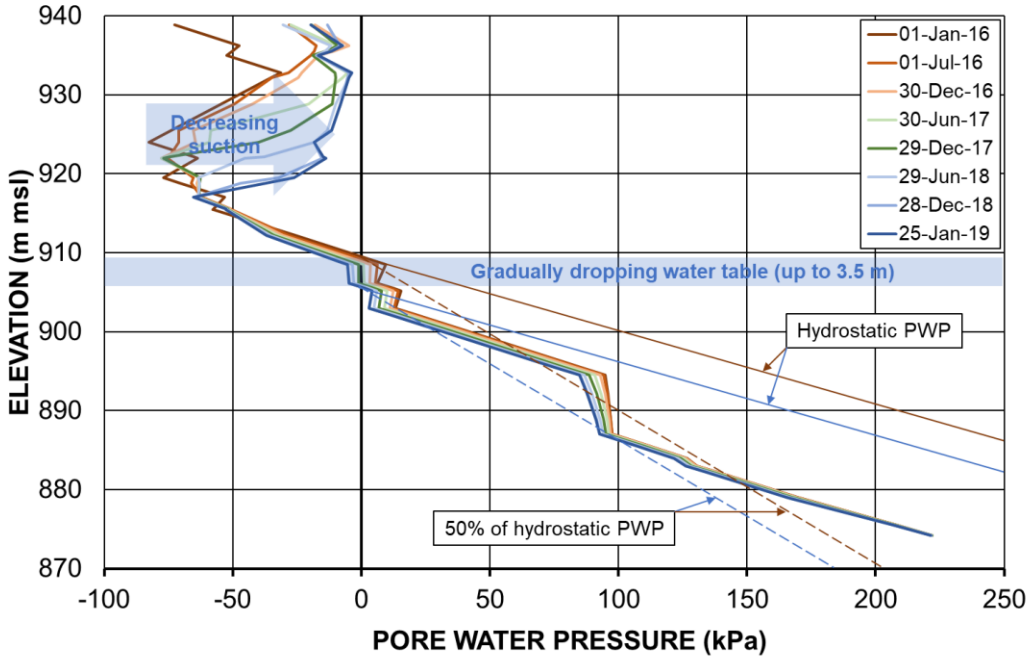

Figure 46: Pore Water Pressure Profile Beside Top Berm on Cross-section 3-3

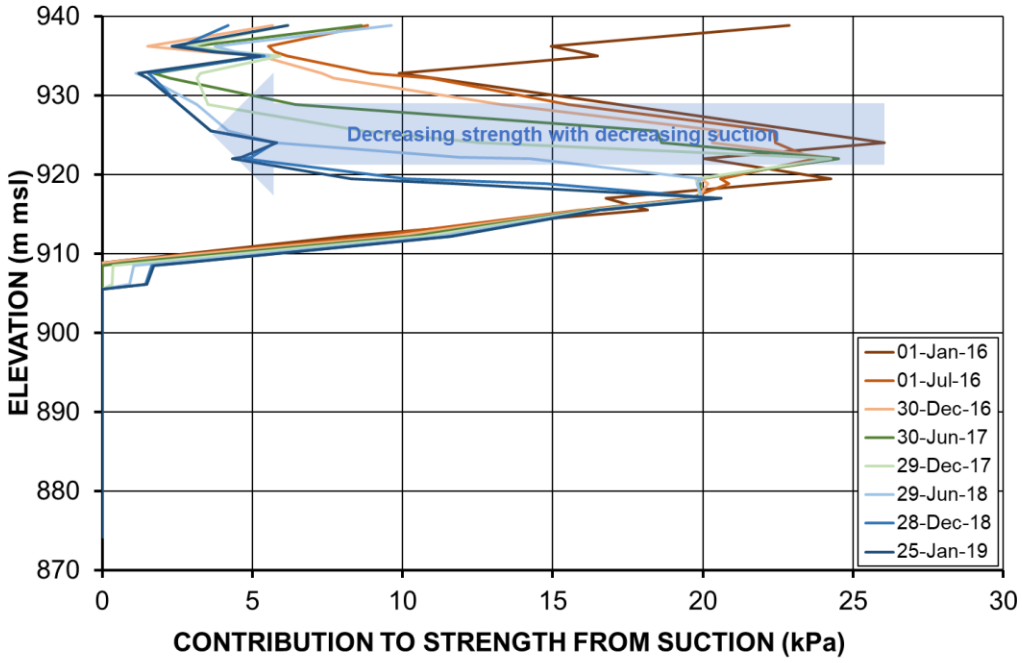

Figure 47: Approximate Contribution of Decreasing Suctions to Shear Strength

5.1.1 Transient 1D Simulation

A 1D unsaturated model was set up to confirm the results of the 2D transient simulation. A profile was taken at the crest of the dam at the same location reported in cross-section 3-3. The primary difference in the 1D model is that 100% of rainfall is applied and evaporation is considered using the Thornthwaite (1948) method to calculate PE and the Fredlund-Wilson-Penman (2000) method to calculate AE. The same time period from January 2016 until the failure in January 2019 was evaluated.

The results (Figure 48) show close similarity to the results of the 2D model, which confirms that wet years caused suctions to be reduced in a zone that moved down through the unsaturated zone and reached a depth of about 25 m after three years. The results also confirm that applying a net infiltration rate equal to 50% of rainfall provided a similar change in suctions compared to the 2D model.

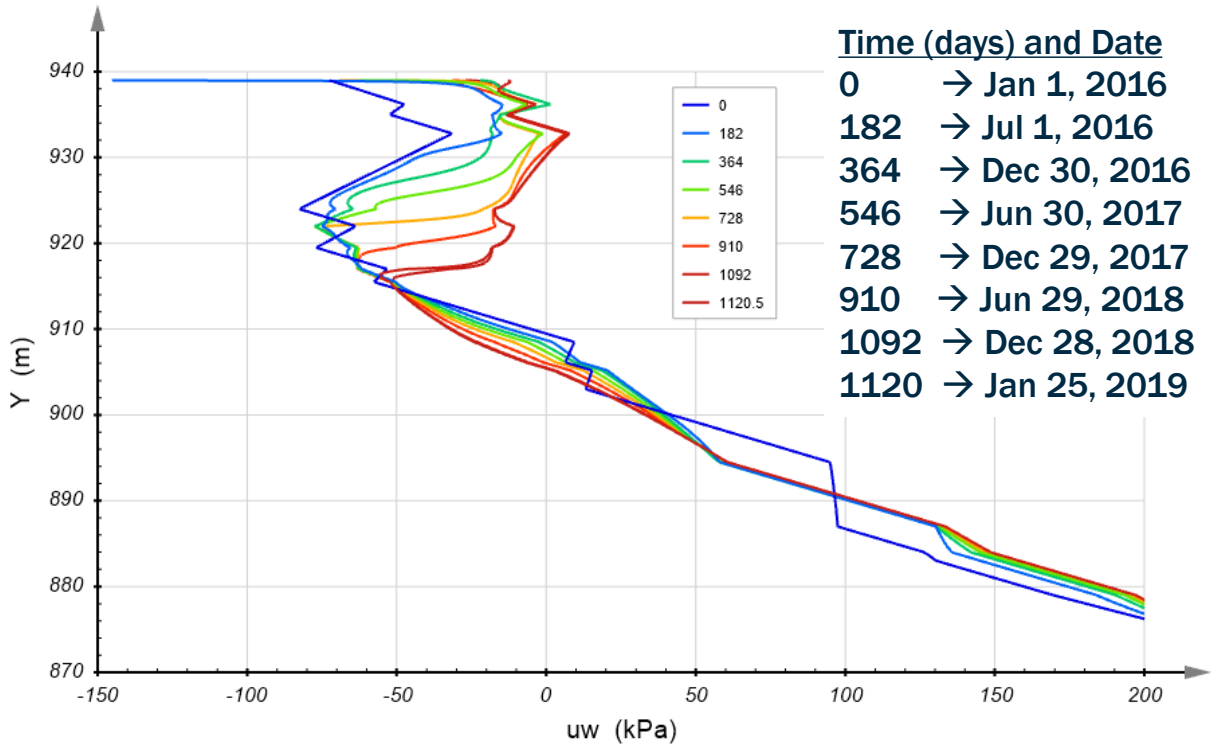

Figure 48: Results of 1D Model Near Dam Crest for Cross-section 3-3

5.2 3D Constructed Stages

This section presents the results of different construction stages based on 3D simulations with 50% rainfall applied on the surface boundary. The construction of the dam consisted of 10 raises and 15 construction stages as illustrated in Figure 7. This section includes the results for selected stages only, particularly for Stage 5 (end of Second Raising construction), Stage 10 (end of Fifth Raising construction), and Stage 15 (end of Tenth Raising construction).

The 3D results at Stage 5 are shown in Figure 49 for a slice taken at cross-section 3-3. Geometry as well as the beach length vary laterally along the dam. Variation in pore water pressure profiles on different sections is expected. For comparison, results from the 2D model are shown in Figure 50 for the same cross-section. The difference between the water daylighting seen in the 3D view and 2D cross-sectional view is because of the materials used in the berms. The First and Second Raisings were mostly covered by the compacted soil (Laterite). The coefficient of permeability of the compacted soil was very low (1.2×10^{-9} m/s, Table 3), which inhibits infiltration due to rainfall. Hence, a very thin zone at the top was wet due to rainfall while the soil underneath still is unsaturated.

The water level in Figure 49 is slightly lower when compared to the water level from a 2D analysis for cross-section 3-3 (Figure 50). The difference in the results can be attributed to the unsaturated material properties used for 2D analysis.

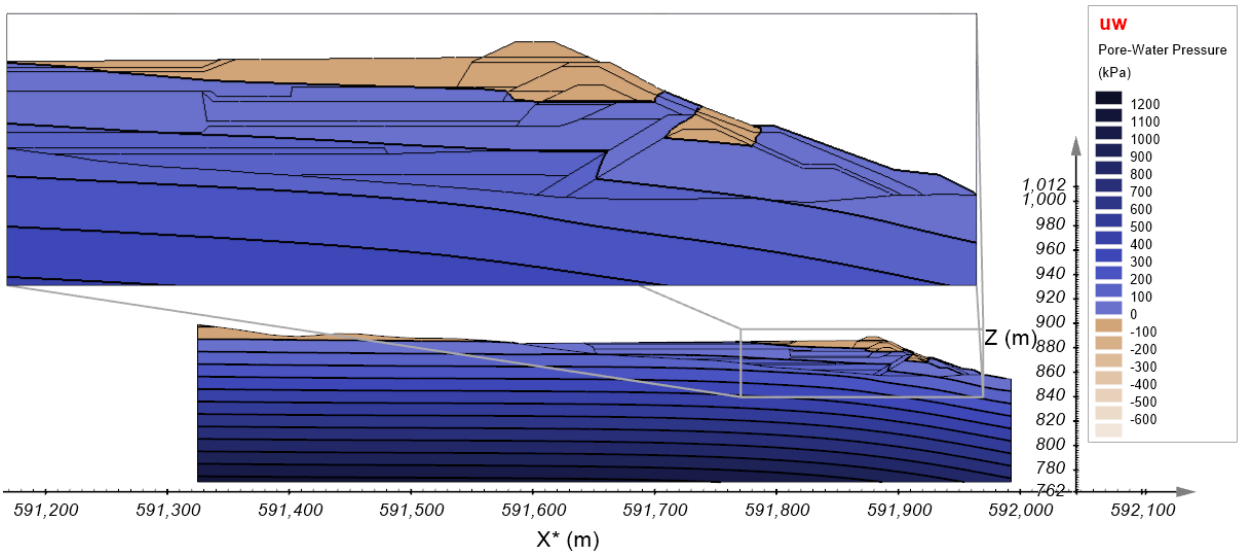

Figure 49: A 2D Profile View Along Cross-section 3-3 of Construction Stage 5 of a 3D Heterogeneous Unsaturated Tailings Model

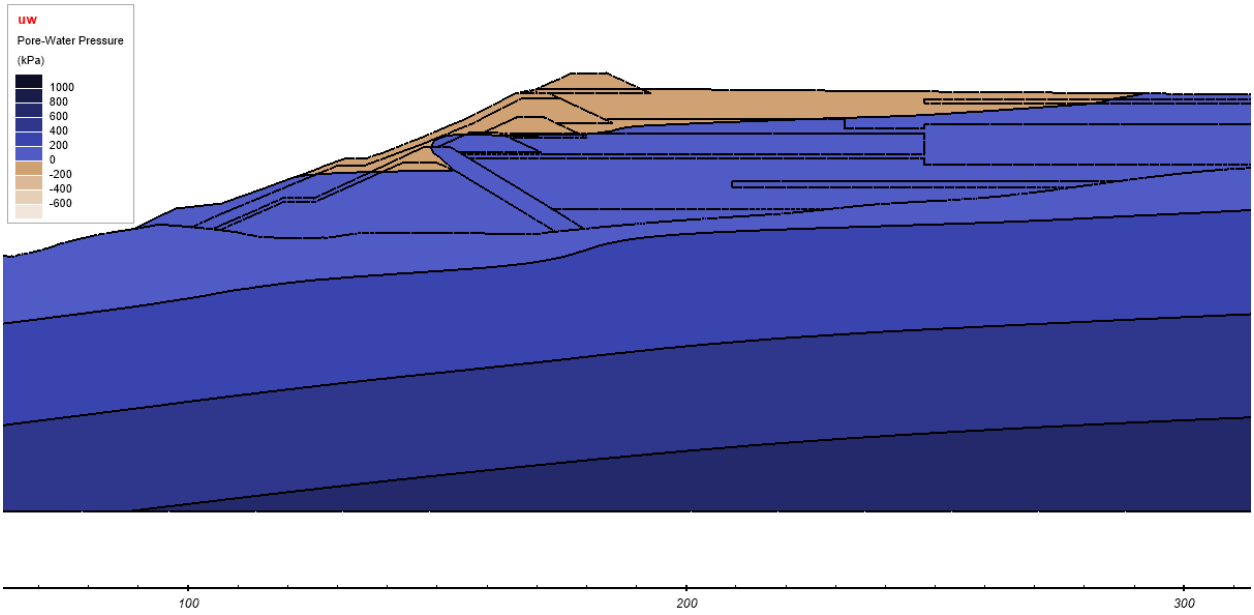

Figure 50: Pore Water Pressure Profile at Construction Stage 5 With Saturated Material Properties in a 2D Analysis

Figure 51 shows the 3D results at Stage 10. At Stage 10, the beach length is larger for cross-section 3-3 as opposed to cross-section 1-1 and cross-section 2-2.

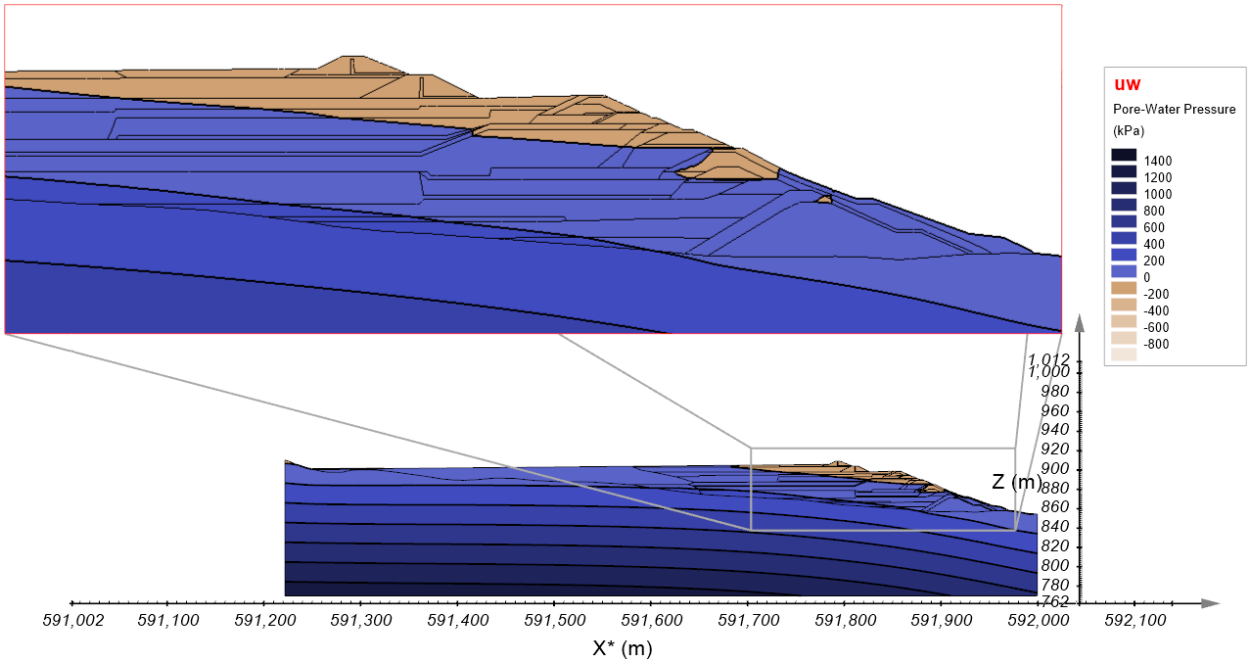

Figure 51: A 2D Profile View Along Cross-section 3-3 of Construction Stage 10 of a 3D Heterogeneous Unsaturated Tailings Model

Stage 15 represents the final raise (Tenth Raising) of the dam completed in January 2016. The pond boundary condition was applied as it was observed close to the start of 2016. Figure 52 shows a slice at cross-section 3-3 and shows that the water table is lower under the upper portions of the dam. This is mainly because of the use of compacted soil material for the Eighth and Ninth Raisings. The compacted soil inhibits the infiltration rate, and only the top surface zone can be saturated due to rainfall.

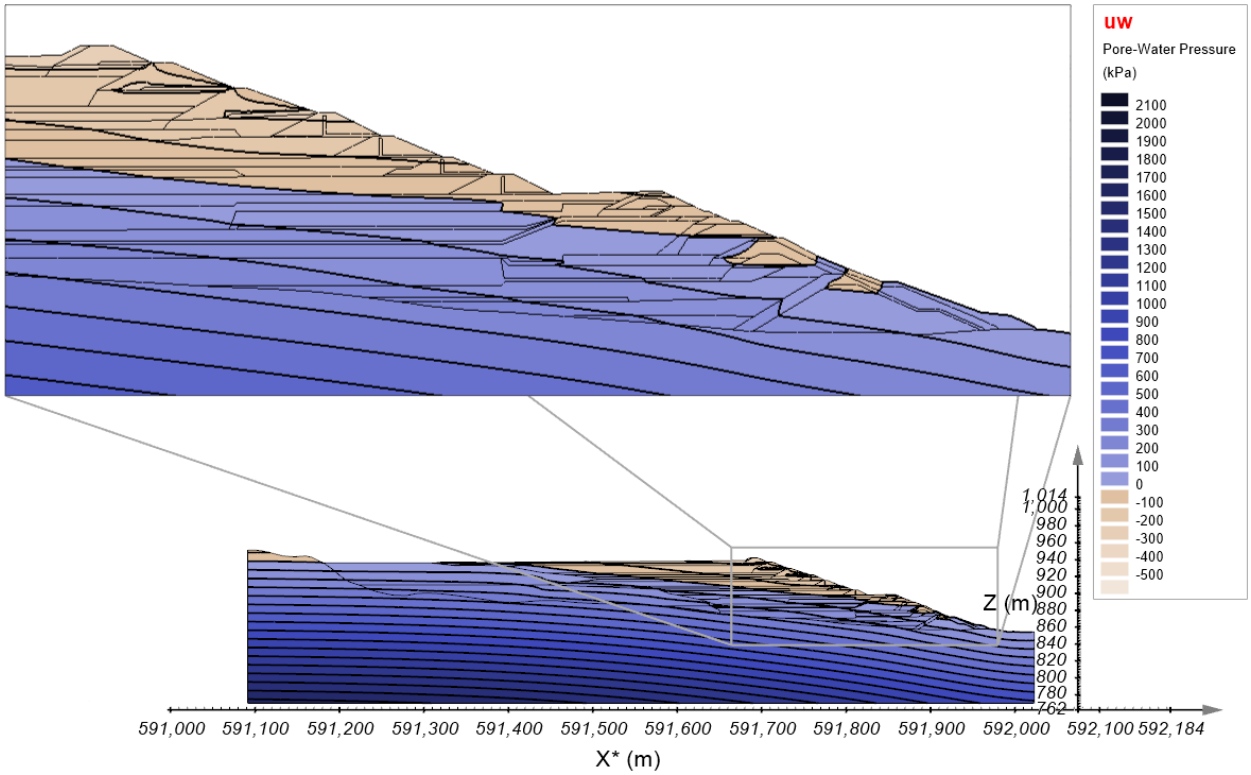

Figure 52: A 2D Profile View Along Cross-section 3-3 of Construction Stage 15 of a 3D Heterogeneous Tailings Model

6 SUMMARY / CONCLUSIONS

The seepage analysis provided the following conclusions:

1. Net infiltration of rainfall was found to be equal to approximately 50% of total annual rainfall.

2. The piezometers did not register short-term climatic events due to the unsaturated zone acting as a buffer.

3. There was a slow decrease in piezometers and INAs in the three years prior to the failure.

4. There was no significant trend in readings during the week leading up to the failure.

5. CPTu dissipation measurements demonstrated a downward gradient of about 50% of hydrostatic. This was confirmed in the transient 1D and 2D seepage models.

6. Climatic events can change suctions that can result in a net average reduction in the shear strength in the unsaturated zone of up to 15 kPa.

The results of the seepage analyses were used to inform and guide the detailed deformation analyses, as discussed in Appendix H.